In-situ observations of wintertime low-altitude clouds over the Southern Ocean

Eunmi Ahn[1], Yi Huang[1,2], Thomas H. Chubb[1], Darrel Baumgardner[3], Peter Isaac[4], Mark de Hoog[5], Steven T. Siems[1,2], and Michael J. Manton[1]

5

Corresponding author: Eunmi Ahn, School of Earth, Atmosphere and Environment, 9 Rainforest

10   Walk, Monash University, Melbourne, Victoria, Australia (jenny.ahn@monash.edu)

[1] School of Earth, Atmosphere and Environment, Monash University, Melbourne, Victoria, Australia

[2] Australian Research Council (ARC) Centre of Excellence for Climate System Science, Monash University, Melbourne, Victoria, Australia

15   [3] Droplet Measurement Technologies, Boulder, Colorado, USA

[4] Ozflux, Melbourne, Victoria, Australia

[5] Entura Hydro Tasmania, Tasmania, Victoria, Australia

1

Abstract

20   Cloud droplet concentration (N_d), effective radius (r_{eff}) and liquid water content (LWC) measured by a DMT CAPS and an SEA WCM-2000 of wintertime low-altitude clouds over the Southern Ocean (SO) are presented for 20 flights taken over three years (June – October, 2013 - 2015). Such clouds have been reported to have the lowest N_d on record (10 - 40 cm^{-3}) from the Southern Ocean Cloud Experiment (SOCEX I) field campaign in 1993. Of the total 20,357 one-second

25   records spent in cloud, 38.5% were found to contain ice crystals, primarily in mixed-phase clouds (36.7%). Ice was observed at some point during 19 of the 20 missions. The droplet spectra and temperature range suggest these clouds were often ideal for the Hallett-Mossop ice multiplication process.

The average N_d and r_{eff} for liquid clouds were 28 ($\pm$30) cm^{-3} and 12.5 ($\pm$2.9) μm, which are

30   consistent with those from SOCEX I. Forty-nine percent of all liquid cloud samples were observed to be drizzling with an average drizzle rate of 0.733 mmhr^{-1}. As drizzle samples were commonly in the neighbourhood of mixed phase or non-drizzling clouds, it was rare to observe solid patches of drizzle of greater than 10 seconds. On average, drizzling clouds had lower N_d and greater r_{eff} and LWC than those of non-drizzling clouds. Distinct observations of non-

35   drizzling clouds with relatively high N_d (~89 cm^{-3}), small r_{eff} (~8.5 μm), and low LWC (~0.173 gkg^{-1}) were noted for two flights. An initial examination of the local environment and synoptic meteorology for these flights failed to identify any particular forcing that may have led to these unique microphysical properties, although these were the only observations of closed mesoscale cellular convection. This research highlights that greater variability exists in the microphysics of

40   wintertime clouds over the SO, when a wider range of synoptic meteorology is investigated.

1.   Introduction

The active and passive remote-sensing capabilities of the A-train constellation have provided unprecedented observations of the macrophysics and microphysics of the clouds and precipitation over the Southern Ocean (SO) for the past decade. These satellite products have provided new measurements of fractional cloud cover and structure (e.g. Mace *et al.,* 2007; Muhlbauer *et al.,* 2014), precipitation (e.g. Berg *et al.,* 2010; Ellis *et al.,* 2009; Wang *et al.,* 2015), and microphysical properties including thermodynamic (or microphysical) phase (e.g. Hu *et al.,* 2010; Huang *et al.,* 2012a). When compared against the North Atlantic or North Pacific, they reveal the unique nature of this remote, pristine environment; the region is dominated by low-altitude clouds (often shallow boundary-layer clouds), which are frequently composed of supercooled liquid droplets. More comprehensive studies (e.g. Huang *et al.,* 2015a) have also highlighted the uncertainty and ambiguity in these satellite products and even inconsistencies between them. These limitations in defining SO cloud properties contribute to the relatively large biases observed in the energy and water budgets of both reanalysis and climate simulations (Trenberth and Fasullo 2010) and can only be resolved with further in-situ observations.

Cloud droplet number concentration (N_d) and effective radius (r_{eff}), necessary for radiative transfer calculations, were two of the first properties examined for SO clouds. Large seasonal cycles in N_d and r_{eff} were observed from the Southern Ocean Cloud Experiment (SOCEX) I and II campaigns (Boers *et al.,* 1996; 1998) with wintertime N_d ranging from 10 - 40 cm^{-3} and summertime N_d ranging from 50 - 180 cm^{-3}. The seasonal cycle was attributed to enhanced marine biogenic activity during the summer season as detailed in the 'CLAW' hypothesis (Charlson *et al.,* 1987; Ayers and Cainey 2007), which takes the first letter of the surname of the hypothesis authors. Quinn and Bates (2011), however, reviewed observations of the individual

steps of this hypothesis and concluded that the sources of cloud condensation nuclei (CCN) over

70 the marine boundary layer were more complex than previously recognised.

With limited recent in-situ cloud observations over the SO, the HIPPO (High-performance Instrumented Airborne Platform for Environmental Research (HIAPER) Pole-to-Pole Observations) campaign (Wofsy *et al.,* 2011) provided a fresh opportunity to examine SO clouds at latitudes as high as 67°S. Chubb *et al.* (2013) examined an April flight in which a lower N_d

75 (30–50 cm^{-3}) was observed in weakly convective stratocumulus in the cold air sector of an extratropical cyclone near 59°S and a higher N_d (80 - 120 cm^{-3}) was observed in homogeneous stratiform clouds at higher latitudes. A wintertime HIPPO flight (Chubb *et al.,* 2016), however, recorded N_d at 100 - 200 cm^{-3}, well outside the range established from SOCEX I. These high concentrations were observed in the midst of gale force pre-frontal winds, far different from the

80 meteorology of SOCEX I missions. It was hypothesized that these winds enhanced the concentration of sea spray aerosols, which in turn contributed to the substantial enhancement of N_d. Huang *et al.* (2015b) included in-situ observations of pristine SO clouds for two wintertime case studies. While the average N_d was consistent with SOCEX I for the first case study (30 - 40 cm^{-3}), it was well outside this range for the second case study (~90 cm^{-3}). Unlike the HIPPO

85 observations, however, the relatively high N_d was not attributed to gale-force winds.

Employing numerical simulations, McCoy *et al.* (2014) concluded that over 50% of the observed spatiotemporal variability in N_d over the SO was tied to sources of natural aerosols. Specifically, variability in N_d was 'driven primarily by high concentrations of sulphate aerosols at lower latitudes (35° to 45°S) and by organic matter in the sea spray aerosols at higher latitudes (45° to

90 55°S)'. Bennartz (2007) employed MODderate-resolution Imaging Spectroradiometer (MODIS) observations of maritime clouds to examine their sensitivity to precipitation, concluding that N_d in non-drizzling clouds was about 2.5 times higher than that in drizzling clouds. Note that

Bennartz (2007) was largely limited to latitudes lower than 45°S and did not account for artefacts

arising from large solar zenith angles (Wood 2012). Wood *et al.* (2012) developed an idealized

95   model of N_d for maritime boundary layer clouds and found that precipitation was a principal

driver of N_d, more so than CCN below the cloud base. Consistent with Bennartz (2007), they

found that the presence of drizzle reduced N_d by a factor of 2 to 3. More recently, Huang *et al.*

(2015b) used spatiotemporal collocated A-Train observations to reveal more distinct

characteristics of the SO clouds, which are sensitive to the presence of precipitation.

100   Precipitation frequency and intensity over the Southern Ocean, especially at mid and higher

latitudes, remain poorly quantified. Wang *et al.* (2015) compared surface observations at

Macquarie Island against nearby CloudSat products, finding that CloudSat products commonly

underestimated the frequency of drizzle and light precipitation. They speculated that CloudSat

might be missing some precipitation from shallow clouds commonly observed at Macquarie

105   Island (Huang *et al.,* 2012b).

The natural variability of N_d and r_{eff} for SO clouds remains poorly understood due primarily to

limited in-situ observations. This work presents in-situ observations of the microphysical

properties of pristine SO clouds from 20 flights over the open ocean around Tasmania, Australia,

taken over the course of three winters (2013-2015). Unlike SOCEX I, observations have been

110   made under a variety of meteorological conditions. In addition to examining the natural

variability of the cloud microphysics, this analysis further examines their sensitivity to the

presence of drizzle.

2.   Methodology and Data

115   **2.1   Flight Overview**

In-situ observations of SO clouds have been made during 20 flights of June – October, 2013 -

6

2015 from a lightly instrumented Cessna Conquest employed by Hydro Tasmania Ltd. (Huang *et al.,* 2014, 2015b). The analysis is limited to in-cloud observations located over the open ocean (43 – 45°S, 145 – 148°E), upwind of Tasmania. These clouds must not have been influenced by any upwind terrestrial sources of aerosols for a minimum of three days as examined with standard back-trajectory calculations (Figure 1) made with the Hybrid Single Particle Lagrangian Integrated Trajectory (HYSPLIT) model (Draxler and Hess 1998) employing the Global Data Assimilation System (GDAS) reanalysis. We refer to such conditions as being 'pristine' and are comparable to the 'baseline' conditions observed at the Cape Grim Baseline Air Pollution Station (CGBAPS) (e.g. Gras 1995), only the wind heading is not strictly constrained due to orography as it is for the fixed site of CGBAPS.

Twelve of 20 flights were 'research-only' flights, fully dedicated to observing 'pristine' SO cloud microphysics. These flights were constrained to coincide with A-Train overpasses, when the aircraft was not being used by Hydro Tasmania for operational cloud seeding (e.g. Morrison *et al.,* 2013, 2010). The remaining eight flights were comprised of 'pristine' segments of select operational cloud seeding flights. While the vast majority of cloud seeding flights were not suitable for this analysis, on very limited occasions the Cessna Conquest flew upwind of any seeding activity, over the open ocean, to collect unperturbed samples that would be suitable for other research activities (e.g. initialising numerical simulations.) These pristine segments often consisted of ferrying out over the water to a point off the coast at which point a sounding was undertaken. We have included the pristine segments from these eight flights, as they satisfy our criteria and thus extend the climatology. The inclusion of these data does, however, introduce another sampling bias towards conditions suitable for operational cloud seeding. In Table 1 we examine this potential bias, finding no substantial difference in cloud effective radius or droplet number concentration between cloud seeding and research-only missions. It is further noted that

seeding was not even undertaken in two of these eight cloud seeding flights. Further details of cloud seeding flights are described in supporting information.

All data are recorded and analysed at a temporal resolution of 1 Hz, which corresponds to a spatial scale of approximately 100 m based on the typical aircraft true air speed. The 20 flights

145   analysed (Table 1) comprise a total of 20,357 one-second cloud samples. The flights of 14 June 2013 and 23 July 2013 have previously been presented in Huang *et al.* (2015a). ~~The remaining eight flights were selected operational cloud seeding flights undertaken by Hydro Tasmania (Morrison *et al.,* 2013, 2010) that included sampling pristine SO clouds.~~

150   **2.2   Aircraft Instrumentation**

Ambient and dew point temperatures are measured with a Meteolabor TP-3S (Meteolabor AG, Switzerland) mounted inside a reverse-flow housing to protect the instrument from hydrometeors. N_d and r_{eff} of liquid water clouds derived from measurements with a Droplet Measurement Technologies (DMT) Cloud, Aerosol and Precipitation Spectrometer probe (CAPS:

155   Baumgardner *et al.,* 2001), which consisted of a hot-wire liquid water sensor (LWC-100), a Cloud Aerosol Spectrometer (CAS) that measures particles from 0.5 to 50 μm, and a Cloud Imaging Probe (CIP) that is used for larger particles from 25 μm to 1.55 mm. For all the calculations, we omit the measurements from the first three bins of the CAS (bin sizes less than ~ 0.68 μm) and the first two bins of the CIP (bin sizes less than ~ 62.5 μm) given the high

160   uncertainties in the measurements. ~~resulting in a range for the CAS of 0.68 – 50 μm and that for the CIP of 100 – 1550 μm. first two bins of the CIP and the 34th bins onward from the CIP due to their high uncertainties, resulting in a range for the CAS of 0.68 – 50 μm and that for the CIP of 62.5 – 837.5 μm.~~ For the CIP data processing, the 'System for Optical Array Probe Data Analysis (SODA)' software developed at the National Center for Atmospheric Research (NCAR) was

165 used. We note that the DMT CAPS was not equipped with Korolev anti-shattering tips (Korolev *et al.,* 2013) for all flights during 2013. As such, a shattering correction (Korolev, 2007), was applied with the SODA software to remove any potential shattered ice particles or artifacts due to splashing of precipitation drops on the tips. The details of the CIP data processing including the 'water processing' and 'shattering correction' are described in the supporting information. ~~As~~

170 ~~such mixed-phase and ice cloud samples from these flights may contain small ice particles from ice shattering. We do not believe that this leads to significant issues as we filtered out mixed and ice phase clouds for calculation of microphysical values. The spectra of liquid water clouds from each flight of 2013 were similar to those of later years with a 'peaked shape' spectra (Figure S2) suggesting that liquid phase water was dominant rather than shattered ice (McFarquhar et al.,~~

175 ~~2013).~~

Bulk liquid and total water concentrations were also measured with a Science Engineering Associates Inc. (SEA) WCM-2000 Multi Element Water Content System (Lilie *et al.,* 2005). The WCM-2000 has two independent hot-wire elements (0.5 and 2 mm) in diameter for liquid water content (LWC) and a scooped 4 mm element for total water (ice + liquid) content (TWC). These

180 three instruments are conventionally called the LWC021, the LWC083 and the TWC156, respectively. Measurement uncertainties and limitations of the WCM-2000 are described in the supporting information.

In this study, cloud was defined by a total water content (TWC) threshold of 0.01 gm^{-3} (Korolev *et al.,* 2003; Wood and Field 2011; Boutle *et al.,* 2014) as measured by the TWC156 and the

185 CAPS (CAS + CIP). Following Korolev *et al.* (2003), liquid water clouds were separated from mixed phase and ice clouds when the ice-water fraction, μ_3, was less than 0.1 with μ_3 defined as $W_{ice} / (W_{liq} + W_{ice})$ with liquid water content (W_{liq}) and ice water content (W_{ice}) derived from measured LWC and TWC from the LWC083 and TWC156. Calculation of liquid and ice water

content is described in detail in the supporting information. Calculations of ice water content

190 (IWC) using LWC and TWC hot-wire instruments have been used in many studies (Mazin *et al.,*

1992; Korolev and Isaac 1998, 2000; and Cober *et al.,* 2000, 2001).

~~All aircraft measurements have been quality controlled.~~ Quality control of the thermodynamic

data (e.g. pressure, temperature and humidity) was performed. Several independent

measurements and derivations of LWC and TWC with the DMT CAS, CIP, LWC-100 and the

195 WCM-2000 were made, and the data were selected when the instruments showed reasonably

comparable results.

3. Meteorology

3.1 Pristine Clouds

200 The meteorology of the Southern Ocean is primarily defined by the circumpolar storm track

(Simmonds and Keay 2000; Hoskins and Hodges 2005). In the vicinity of Tasmania and

southeast Australia, cold fronts are commonly anchored in mid-latitude cyclones and cut-off

lows and they are the main cause of wintertime precipitation (Risbey *et al.,* 2009; Chubb *et al.,*

2011). Commonly, pristine conditions are encountered to the west and south of Tasmania during

205 post-frontal periods that can last for one to four days. In the space between cold fronts, a mid-

latitude ridge often becomes the dominant synoptic feature. This feature can also force pristine

SO air mass towards Tasmania, especially when the ridge is present to the west of Tasmania.

The majority of the SOCEX I flights (Boers *et al.,* 1996, 1998) were conducted when such a

ridge was prominent and produced a well-defined boundary layer with boundary layer clouds. In

210 contrast to the SOCEX I flights, operational cloud seeding flights are typically flown shortly

after the passage of the cold front (6-24 hours) when supercooled liquid water is readily

encountered at much higher elevations (up to 4 km) (Morrison *et al.,* 2010). The research flights

were not constrained by the meteorology, although no flights were conducted in the midst of a cold front due to a potential of lightening hazard. Table 1 details the dominant synoptic features for each flights.

When the observations were limited to low to mid-level clouds only, it was also possible to identify the structure of the mesoscale cellular convection (MCC) (if any) following Wood and Hartmann (2006). MODIS visible and infrared images with a time window as close as the flight time were employed for this classification (Table 1). Most of the observations made shortly after the passage of a cold front are found to be of open MCC. Muhlbauer *et al.* (2014) illustrated that during winter open MCC occurs relatively frequently in the lower latitudes of the SO. This is opposed to the closed MCC, more commonly found when a high pressure ridge is the dominant meteorological feature, as observed during SOCEX I.

Table 1 also details the average thermodynamic characteristics (cloud phase fractions, temperatures, pressures) of the clouds sampled for all 20 flights. While the aircraft did, on occasion, observe mid-level clouds with average pressures as low as 667 hPa, the vast majority of observations were made in low-level cloud (pressures greater than 700 hPa), as detailed in Figure 2 (a). The average in-cloud temperature reveals that the pristine segments of operational cloud seeding flights spent the majority of time ferrying in clouds between -8 and -10 °C; research flights observed clouds over a far greater range of meteorological conditions, although the temperature range was commonly between -6 and 0 °C.

Estimated cloud top and base heights are also presented in Table 1, as recorded during the aircraft sounding on site. We note, however, that these observations may be of limited value given that the clouds did not reside in horizontally homogeneous fields, especially for open and disorganised MCC. Observations of cloud top height, cloud base and cloud thickness often varied substantially over the course of an hour.

3.2 Cloud Thermodynamic Phase

Table 1 further details the time spent in cloud for each flight. Using the ice-water fraction, μ_3, the

240 cloud samples were sorted in 'liquid' clouds ($\mu_3 \leq 0.1$), 'mixed phase' clouds ($0.1 < \mu_3 < 0.9$) and

'ice' clouds ($0.9 \leq \mu_3$), following Korolev *et. al* (2003). The percentage of time spent in these

conditions is presented for each flight along with the percentage over all 20 flights. Overall, ice

clouds were only sampled 1.8% of the time but mixed phase clouds were encountered 36.7% of

the time. 19 of the 20 flights recorded the presence of ice (mixed-phase or ice) at some point in

245 these pristine clouds over the open ocean, which is a very different picture from that illustrated

by SOCEX I. Boers *et al.* (1996) lists a single flight that encountered mixed phase clouds, which

was subsequently removed from the analysis. Not surprisingly, the percentage of time in liquid

clouds is correlated with the average in-cloud temperature; liquid clouds are more common at

warmer temperatures, and mixed-phase and ice clouds are more common at colder temperatures

250 including the range of -3 and -8 ℃ necessary for the Hallett-Mossop process of ice multiplication.

The sensitivity of the ice-water fraction, μ_3, to the ambient temperature can be explored in a

means similar to Korolev *et al.* (2003) (Figure 2). All in-cloud observations were sorted into 5

℃ bins. At temperatures greater than 0 ℃, clouds are predominantly liquid with μ_3 always less

than 0.1. At temperatures between 0 ℃ and -5 ℃, μ_3 is less than 0.1 roughly 76% of the time

255 with much of the remaining cloud having at small values ($0.1 < \mu_3 < 0.5$). At colder temperatures

(-10 ℃ < T < -5 ℃ and -15 ℃ < T < -10 ℃), the frequency of liquid clouds drops to less than

40% while mixed phase samples ($0.3 < \mu_3 < 0.7$) become dominant. Heavily glaciated clouds (μ_3

> 0.7) are rarely encountered at any of the temperature bands. As discussed before, heavily

glaciated clouds may be under sampled in this study as deep, frontal clouds were intentionally

260 avoided in both the research and operational cloud seeding flights. Nevertheless, such

distributions are notably different from those reported in Korolev *et al.* (2003) where observations were taken from five different field campaigns across Canada although instrumentation and time in clouds were different from ours. The mixed phase clouds sampled across Canada were found to be primarily liquid or primarily glaciated with a minimum for $0.2 < \mu_3 < 0.7$ for temperature bands below 0 °C. For the -15 °C < T < -10 °C temperature band, ice clouds were observed nearly 40% of the time in the Canadian flights opposed to ~1% for the pristine SO clouds examined in our study. Such differences in ice fractions support the argument of Burrows et al. (2013) that there are fewer active ice nuclei over the Southern Ocean at these temperatures.

4. Liquid clouds

4.1 Mean Microphysical Characteristics

Hereafter we limit our attention on liquid clouds ($\mu_3 \leq 0.1$) only when considering r_{eff}, N_d and liquid water content (LWC). Accordingly, the number of cloud samples is reduced from 20,357 to 12,520. The average for each individual flight (representative average) in Table 1 is calculated following Boers *et al.* (1998), which first averages r_{eff} and N_d separated into 10 hPa pressure bands. The values in each pressure band are then averaged to define the representative average. The first two rows in Table 2 are calculated from the 20 representative averages and are comparable to those reported for SOCEX I. A simple time average N_d from all 1-second liquid cloud samples from all flights is 28 cm^{-3} with a standard deviation of 30 cm^{-3} (Table 2). The SOCEX I wintertime range for N_d (10 – 40 cm^{-3}) holds for 17 of the 20 flights (Table 1). One flight (03 Aug 2013) recorded a lower average N_d of 7 cm^{-3}, and the remaining two flights recorded N_d at 80 and 89 cm^{-3}, respectively. The liquid clouds sampled for the low N_d flight (3 Aug 2013) may be anomalous in that they were relatively cold and sparse. The majority of the

285 clouds encountered on this day were mixed-phase (79.1%). The observations from the two high

N_d flights (denoted as CASE A for 23 Jul 2013 and CASE B for 01 Oct 2015), however, are

believed to be robust. They are also unique, being the only encounters of closed MCC and are

examined in more detail in the next section. When sorted by MCC structure, the difference

between open and closed MCC clouds is evident (Table 1). The two remaining classes

290 (unorganised and no structure) have microphysical properties much closer to open MCC than

closed MCC clouds.

Turning to the effective radius (CAS only), the average over all liquid cloud samples (Table 2,

simple average) is 12.5 μm with a standard deviation of 2.9 μm, with 18 of the 20 flights having

r_{eff} in the range of 9.8 to 15.4 μm. These values are comparable to those reported for SOCEX I.

295 The two high N_d flights have the lowest values of r_{eff} (CAS) at 8.2 and 8.5 μm (Table 1). When

the larger droplets from the CIP are included, the average effective radius over all liquid cloud

samples, r_{effT}, increases to 21.6 μm with a standard deviation of 25.7 μm. The average liquid

water content (CAS + CIP) is 0.278 gkg^{-1} with a standard deviation of 0.956 gkg^{-1}. The two high

N_d flights had relatively low LWCs (CAS+CIP) at 0.173 and 0.165 gkg^{-1}, respectively.

300 It may be argued that these average liquid cloud properties may not represent ideal liquid clouds

given that mixed phase samples are intermixed on numerous flights. This is explored by

recalculating the properties after filtering out any liquid cloud observations that are near (within

five minutes) a mixed phase or ice sample, leaving only isolated liquid cloud samples from eight

"consistent-liquid" flights (Table 2). The two high N_d flights are included in these eight. Overall,

305 the total number of 1-second liquid cloud samples was reduced from 12,520 to 3,258. The

average N_d increases to 40 cm^{-3} with a standard deviation of 41 cm^{-3}, as the two high N_d flights

were largely retained in this calculation. The effective radius dropped to 11.4 (±3 μm) for the

CAS-only, and 22.4 (± 28.2 μm) for the CAS+CIP calculation. The LWC (CAS+CIP) increased

to 0.227 (±0.590 gkg^{-1}). This information is summarised in Table 2 along with comparable

averages from SOCEX I (Boers *et al.,* 1996), although it was not possible to analyse the four

'baseline' flights of SOCEX I in an identical manner.

It is also of interest to test the sensitivity of these values to the ambient temperature. Much like

the analysis of the ice-water fraction, these liquid cloud properties are now sorted into

temperature bands of 5 °C from -15 °C to 10 °C (Figure 3). The liquid only cloud samples of all

20 flights (12,520 one-second samples) have been compiled for these calculations.

Approximately 73% of all samples were in the two bands between -5 and 5°C. Approximately

6% of the samples were from clouds warmer than 5 °C and 20% of the samples were at

temperatures below -5 °C. This sharp drop in fractional cloud cover at colder temperatures is

consistent with the climatology of Huang *et al.* (2012b) using satellite observations.

When the liquid cloud observations are aggregated in this manner, there is no significant

difference in N_d and r_{eff} of clouds from -10 to 5 °C. Despite the large variability, warmer clouds

(5 °C < T < 10 °C), presumably lower elevation clouds, tend to have greater values of N_d, and

colder clouds (-15 °C < T < -10 °C) have lower values of N_d (Figure 3). When the effective

radius is calculated from only the CAS probe, r_{eff}, no significant variation is observed over

different temperature bands. If, however, the CAS+CIP effective radius, (i.e. r_{effT}) is used, then a

positive trend is observed with increasing temperature. We suspect that this trend is largely a

reflection of drizzle developing in these clouds as drizzling clouds have a higher portion of large

(greater than 15 μm) r_{eff} (CAS+CIP), as shown in Figure 4(b) which is described in section 4.2.

~~LWC remains relatively steady at 0.13 gkg^{-1} for temperatures greater than -10 °C, with the~~

~~CAS+CIP LWC being ~20% greater than that of the TWC probe. As noted in the supporting~~

~~information, this may be due to oversizing out of focus drops. An overestimate of 10% in drop~~

~~size will lead to about a 20% bias in LWC. Some undersizing of larger droplets by the WCM-2000, however, cannot be ruled out.~~ The LWC (CAS) is between 0.13 – 0.2 gkg-1 for temperatures greater than -10 °C, with very little LWC differences from the CAS+CIP and TWC probe. This confirms that ~20% over-estimation from the CIP LWC from out of focus effects is well corrected by Korolev (2007) as described in the supporting information.

Similar to the bulk measurements, the spectra of particle size from the CAS and CIP measurements can be aggregated into 5 °C temperature bands (Figure 3 (d)). The warmest clouds have the largest contribution of small droplets (D_p < 10 μm), while the coldest clouds have the fewest in this range. If drizzle developed in the warmest clouds, then we might expect the small droplets to be removed by coalescence. This large contribution of small droplets at warmer temperatures actually reflects the relative contribution of the two high N_d flights, in which much of the cloud sampled was at warmer temperatures (Table 1).

Focusing on larger droplets and drizzle, some variation is evident at the extreme temperature bands; at the colder temperatures, a strong drop off is evident in the number of larger drops (D_p > 200 μm), perhaps suggesting an absence of drizzle in these clouds. At warmer temperatures a drop off is evident in the number of droplets between 20 and 200 μm. Not surprisingly, the LWC is largely defined by the drops over 20 μm but less than 200 μm (Figure 3 (e)). Only the clouds at the warmest temperatures show a significant contribution to LWC from the drops greater than 500 μm.

4.2   Drizzle/Light precipitation

As noted in Wood *et al.* (2012), the presence of drizzle can modify the cloud microphysics. Precipitation, even light drizzle, can result in the removal of smaller cloud droplets by collision and coalescence. In general, precipitation may leave clouds with smaller values of N_d and larger

r_{eff}, or clouds with small r_{eff} are less likely to contain drizzle (Rosenfeld *et. al*, 2012). It is an open question as to whether precipitation drives to the very low values of N_d observed over the Southern Ocean. Boers *et al.* (1996) encountered active drizzle on some of the SOCEX flights and speculated that the other 'baseline' clouds had previously experienced light precipitation due to low N_d and sub-adiabatic LWC. Here we employ the CIP to define the presence of drizzle. For a liquid cloud, if the LWC from droplets with size greater than 112.5 μm is greater than 0.005 gm^{-3} in clouds, then the sample was classified as drizzling. Rain rate was calculated using the fall speed of those droplets (Pruppacher and Klett 2010). As our flights avoided active cold fronts, our samples are primarily of drizzle or light precipitation. Further, mixed phase clouds are excluded in this analysis, although it is likely that the majority of these samples would be classified as being precipitating.

Overall, the liquid clouds observed in this study were drizzling 49% of the time (9975 samples, Table 1) and their mean rain rate was 0.733 mmhr^{-1}. The percentages for drizzle and rain rates for individual flights are also detailed in Table 1, which range from 100% to 0% and 3.667 mmhr^{-1} to 0 mmhr^{-1}, respectively. ~~The rain rate for these observations is conservative due to the 835 μm droplet size threshold being used on the CIP measurement.~~ In Table 3 the standard cloud properties have been recalculated based on the detection of drizzle. The average N_d of 'drizzling' liquid clouds drops to 26 (± 18) cm^{-3} and, correspondingly, the average in 'non-drizzling' clouds increases to 36 (± 36) cm^{-3}. The two high N_d flights contribute substantially to the non-drizzling clouds. Not surprisingly, the effective radius (CAS only) is larger for drizzling clouds (13.5 ± 2.5 μm) than that for non-drizzling clouds (10.6 ± 3.5 μm). Liquid water content is higher in drizzling clouds (0.185 ± 0.179 gkg^{-1}) than non-drizzling clouds (0.126 ± 0.151 gkg^{-1}). These differences are statistically significant according to K-S tests and T-Tests with *p*-values approaching 0 for N_d, r_{eff}, and LWC.

17

380　Given that drizzle was highly intermittent in these clouds, the data were further sampled to only consider 'solid patches' of drizzle, i.e. liquid cloud samples where drizzle was detected for at least 10 seconds. Similarly, 'solid patches' of non-drizzling clouds could be defined. We found that this refinement had a very minor effect on the average properties of drizzling clouds and a minor effect on the non-drizzling clouds (not shown). The ambient temperature of the samples

385　was also averaged according to the presence of drizzle. While there is considerable variability, we note that on average drizzling clouds were warmer (-0.9° ± 4.4°C) than non-drizzling clouds (-3.8° ± 5.6°C). This temperature difference is statistically significant. This difference may be due to drizzle being at a more mature/advanced state at lower altitudes or warmer temperatures.

In Figure 4(a), all 12,520 liquid cloud samples have been sorted into bins according to N_d to

390　produce a probability density function (PDF). The bulk of the 1-second observations (~83%) have N_d less than 45 cm^{-3} and are split roughly equally between drizzling (49%) and non-drizzling (51%) samples. Only ~11% of the samples have N_d between 45 and 75 cm^{-3}, with little difference between drizzling and non-drizzling. Less than 5% of all samples have N_d between 75 and 105 cm^{-3}. Approximately 5% of all samples have N_d between 105 to 120 cm^{-3}, and these

395　were almost exclusively from the two high N_d, non-drizzling flights. It is not possible to establish whether any of the non-precipitation observations are being sampled after they experienced precipitation. However, like the conclusions of Boers *et al.* (1996), we similarly speculate that if N_d is less than 45 cm^{-3} for a non-drizzling cloud, then it is likely to have already experienced drizzle. For N_d greater than 105 cm^{-3}, however, we assume that the non-drizzling cloud has not

400　experienced any drizzle even though there is no direct means to observe this or infer the age of clouds.

Similarly, a PDF (Figure 4(b)) can be produced for the combined effective radius, r_{effT} (CAS + CIP), with the fractional contribution much as expected; non-drizzling clouds generally have

smaller effective radii. Almost none of non-drizzling samples had an effective radius greater than

405   20 μm. Consistent with Table 1, ~67% of all one second samples have r_{effT} between 5 and 30 μm.

Drizzling clouds dominate the contribution to average effective radius when r_{effT} was greater than

15 μm. This carries forward to the LWC (Figure 4(c)), reflecting the greater contributions of the

large CIP droplets to this measurement. Non-drizzling samples are only dominant for thin/light

clouds (LWC < 0.1 gkg^{-1}), although even these thin clouds can experience drizzle. The spectra

410   for drizzling and non-drizzling clouds are as expected (Figure 4 (d)). In general, drizzling clouds

have a greater concentration of larger droplets and a reduction of smaller ones (size < 10 μm).

It is interesting to examine the intermittency of drizzle (and non-drizzle) in these SO clouds

which is indicated by the frequency of the duration of drizzling and non-precipitating 'patches'

(Figure 5). This is important because many satellite retrieval algorithms assume some kind of

415   horizontal homogeneity. Drizzle and non-drizzle patches of short one and two second durations

(equivalent to ~100 to200 m) are most common. It was quite rare to observe solid segments of

non-precipitating clouds for periods of greater than 10 seconds (1 km). While it was more

common to observe this for drizzling clouds, it was still relatively rare. This may be due to a

combination of the small size of these clouds (which are primarily open MCC and unorganised

420   MCC) and the intermittent presence of mixed-phase and glaciated samples, as well as intermixed

drizzling and non-drizzling samples, all of which lead to a high degree of inhomogeneity.

Stretches of relatively homogeneous boundary layer cloud simply were not observed in these 20

fights except in CASE A, which is further examined in Section 5.

425   **5.   A Comparison of Drizzle and Non-Drizzle Cases**

Overall, the average cloud properties examined in this study were very consistent with those

established during SOCEX I. Pristine liquid wintertime clouds over the SO have a low droplet

number concentration, large effective radius and, given their shallow depth, substantial LWC compared to those in the Northern Hemisphere (Han *et al.,* 1998; Isaac *et al.,* 2001; Gultepe and

430   Isaac 2002; Dong and Mace 2003). Further, drizzle is quite common. Looking at the flights individually, two of the 20 flights fail to conform to this picture. The flights of 23 July 2013 (CASE A) and 01 October 2015 (CASE B) were characterised by relatively high N_d, small r_{eff} and very little drizzle (Figure 6). It may be claimed that these two flights 'distorted' the average properties of non-drizzling and warm clouds. If these two flights were removed from the

435   analysis, the differences between 'drizzling' and 'non-drizzling' samples were relatively weak; the r_{eff}, N_d and LWC (CAS + CIP) for the remaining non-drizzling samples were 11.5 μm, 23 cm^{-3} and 0.128 gkg^{-1}, respectively (not shown).

Further, CASES A and B were the only two flights that encountered closed mesoscale cellular convection (Table 1). It is of particular interest to appreciate not only how frequently such clouds

440   exist over the SO, but also the synoptic and mesoscale processes that drive them. As a point of contrast, two 'typical' drizzling flights have been selected, which display low N_d, large r_{eff} and near constant presence of drizzle. The flights of 28 June 2013 (CASE C) and 30 August 2015 (CASE D) were research flights that encountered prolonged periods of lightly precipitating clouds (85 and 91%, respectively), low N_d and large r_{eff}. All four flights were primarily within

445   relatively warm, low elevation clouds.

Table 4 details the local environment for the four flights, as observed by the aircraft. It is difficult to isolate any extreme conditions amongst these four flights. All four flights sampled low-elevation clouds of 500 - 600 m thickness with cloud top ranging from 1 to 1.3 km. The boundary layer clouds of the two high N_d flights were in particularly warm environments. ~~While~~

450   ~~the wind speed for one of the high drizzle flights (CASE C) was observed up to 42 ms^{-1}, the three~~ ~~remaining flights had relatively typical or weak wind speeds.~~

Figure 1 details the back-trajectories of these four flights. An initial inspection does not portray any immediate reason for the anomalous conditions. The high drizzle flight CASE D (30 August 2015) stands out for having an air mass origin from much higher latitudes. By contrast the high

455   drizzle flight CASE C is unremarkable, having stayed in a mid-latitude band. Compared to many of the other back-trajectories this air mass is moving relatively slowly across the Southern Ocean, consistent with the local wind speed measurement. The back-trajectories for the two high N_d flights are also relatively unremarkable. Arguably CASE A air mass was moving slowly, presumably due to the high pressure system, while CASE B air mass was moving relatively

460   quickly.

The daily meteorology was synchronised to these back-trajectories to examine the potential role of fronts and cyclones. In particular, we examined whether either high N_d case encountered gale-force winds as described in Chubb *et al.* (2016), or pre-frontal conditions. Chubb *et al.* (2016) detailed observations of extremely high N_d (200 - 300 cm^{-3}) for the SO, and attributed the

465   observations to sea spray driven from pre-frontal gale force winds. No such conditions were encountered over 72 hours for CASES A and B.

The synoptic meteorology of CASE A flight is more fully presented in Huang *et al.* (2015a). In summary, an intense anticyclone (1,034 hPa) was located near the coast of South Australia with a ridge extending to the southeast to roughly 50°S, 155°E. A small cut-off low was located in the

470   Tasman Sea. The relatively unique conditions drove air from higher latitudes towards Tasmania. A Cloud-Aerosol Lidar with Orthogonal Polarization (CALIOP) overpass and MODIS image found that the free troposphere was largely free of clouds to the south of Tasmania, but solid boundary layer clouds persisted with a cloud thickness of roughly 0.4 - 0.6 km.

Conversely, the high N_d CASE B occurred in post-frontal conditions with a thick layer of clouds

475   between 530 and 650 hPa (Figure 7), as shown by the aircraft sounding. A solid deck of low

21

elevation clouds (pressure > 800 hPa) was also present that day and was the source of the high N_d

samples. The upper layer clouds consist of 51% of mixed and ice phase and the lower layer is

predominantly liquid phase of 98%. A MODIS image for the day reveals the complexity of the

cloud field arising from the passage of a cold front. ~~Looking past the mid-level cloud, the~~

480   ~~relatively small patch of closed mesoscale cellular convective clouds is evident~~. Below the mid-

level cloud, closed mesoscale cellular convective clouds formed over a region of ~ 250km X

~200km. Ultimately, the synoptic meteorology of these two high N_d flights has little in common.

~~even though we do not have the measurements of vertical velocity, which makes our exploration~~

~~of the synoptic conditions and boundary layer dynamics limited.~~

485   The differences in the synoptic meteorology of the two high drizzle flights are much smaller than

that for the high N_d flights. The MODIS images for CASE C and CASE D detail open mesoscale

cellular convection to the southwest and south of Tasmania, respectively. The aircraft sounding

for CASE C identifies an inversion at 820 hPa with a cloud deck extending down to 900 hPa.

The mean-sea-level pressure (MSLP) analysis (not shown) suggests that a weak ridge was

490   dominant over the region for this period of time. These boundary layer clouds were far removed

from any frontal dynamics during the observation period. The aircraft sounding for CASE D

identifies an inversion at 810 hPa with shallow cloud and relatively thicker cloud between 860

and 900 hPa. The MSLP analysis (not shown) displays a cut-off low (1001 hPa) present near

40°S, 158°E, and a strong high pressure system (1033 hPa) south of Tasmania (50°S, 145°E),

495   leaving the Southern Ocean with a southerly airflow. Vertical profiles of cloud microphysical

properties that correspond to the sounding profiles in Figure 7 are shown in Figure 8. Despite the

high variability, it is evident that both average LWC and r_{eff} (CAS+CIP) for the two non-

drizzling flights (CASE A and B) appear to increase with altitudes, which is consistent with a

typical cloud profile described by an adiabatic cloud model. The profiles for the two drizzling

500   flights (CASE C and D), on the other hand, behave differently. In particular, the r_{eff} (CAS+CIP)

for CASE C and D (where heavy drizzle was present) increase dramatically towards cloud base

(warmer temperatures), which is in support of our speculation on the positive trend with

increasing temperature as seen in the climatology (Figure 3(b)). These profiles also suggest that

the drizzling clouds are much more inhomogeneous than the non-drizzling clouds.

505   In summary, an initial investigation into these four cases finds that the synoptic conditions were

not able to fully explain the generation of drizzle and the associated differences in N_d and r_{eff}.

More dedicated in-situ observations and analysis are needed to further explore this issue.

6.   Discussion and Conclusions

510   The microphysics properties retrieved from the SOCEX I (Boers *et al.,* 1996) have long defined

the wintertime climatology of very low N_d ($10 < N_d < 40$ cm^{-3}) and large r_{eff} ($10.8 < r_{eff} < 14.7$

µm) for the liquid clouds of this region. The maximum LWC for these flights was between 0.1

and 0.2 gkg^{-1}. Such pristine conditions are unique in comparison with those of the North Pacific,

North Atlantic or Arctic. For example, during the First International Satellite Cloud Climatology

515   Project (ISCCP) Regional Experiment-Arctic Cloud Experiment (FIRE.ACE), the mean N_d over

the Arctic Ocean in April for clouds of an air mass of Arctic origin was observed at 91 (±43) cm^{-3}

where the temperature was between -25 and 0 ℃ with LWC 0.066 (±0.042) gm^{-3} (Gultepe and

Isaac, 2002). Gultepe and Isaac (2002) detailed observations of air masses of North Pacific origin

with a mean N_d of 57 (±41) cm^{-3}, LWC of 0.14 (± 0.128) gm^{-3}, and r_{eff} of 9.2 (± 4.6) µm in the

520   same temperature range.

Ultimately only five flights taken over four days underpin the SOCEX I wintertime climatology.

Further, those flights were all made under a very specific synoptic setting, namely along the

leading edge of anti-cyclonic ridges, which are commonly observed between the passages of cold

fronts. The ridge largely inhibits mid-level cloud and establishes a well-defined boundary layer

525   inversion. In this work we greatly expand the wintertime climatology of SOCEX I by analysing

observations taken across a much broader representation of the meteorology; pre-frontal, post-

frontal, and near frontal environments have also been sampled. In all, 20 flights taken over the

course of three winters (June – October, 2013 - 2015) have been analysed. Liquid clouds were

sampled up to heights of 5000 m, although this was relatively uncommon.

530   One immediate difference between this campaign and SOCEX I was the common presence of ice.

14 of the 20 flights had ice (either mixed phase or glaciated) present for at least 10% of all cloud

samples. During SOCEX I only one flight observed mixed phase clouds, which was

subsequently removed from any analysis. Of the total 20,357 one-second records spent in cloud

in our observations, 38.5% were found to contain ice crystals, primarily in mixed-phase clouds

535   (36.7%) rather than glaciated clouds (1.8%). The droplet spectra and temperature range suggest

these clouds were ideal for the Hallett-Mossop ice multiplication process, which should come as

no surprise, as this is the region where Mossop first encountered such clouds (Mossop *et al.,*

1970). The mixed phase samples observed commonly had an ice water fraction (μ_3) between 0.5

and 0.7, which is vastly different from those found in the neighbourhood of Canada as detailed in

540   Korolev *et al.* (2003). These mixed phase and glaciated observations are not the primary focus of

this study, leaving the analysis centred on liquid cloud observations.

Ultimately the mean microphysical properties from this new campaign remain consistent with

those of SOCEX I; the average N_d was 28 ($\pm$30) cm^{-3}, the average r_{eff} (CAS only) was 12.5

($\pm$2.9) μm, and the average LWC (CAS+CIP) was 0.278 ($\pm$0.956) gkg^{-1}. When the clouds were

545   filtered to remove those near mixed-phase or glaciated samples (within 5 minutes or ~30 km),

the average N_d was 40 ($\pm$41) cm^{-3}, the average r_{eff} (CAS only) was 11.4 ($\pm$3.0) μm, and the

average LWC (CAS+CIP) was 0.227 ($\pm$0.590) gkg^{-1}.

Similar to SOCEX I, drizzle or light precipitation was frequently observed throughout this campaign. 49 % of all liquid cloud samples were observed to be precipitating. As drizzle samples

550 were commonly in the neighbourhood of mixed phase or non-drizzling cloud samples, it was rare to observe solid patches of drizzle of greater than 10 seconds. ~~It is an open question as to how important mixed phase processes are to the formation of precipitation in these relatively shallow boundary layer clouds.~~

There were distinct observations of non-drizzling clouds with relatively high N_d (~89 cm^{-3}) and

555 small r_{eff} (~8.5 μm) for two of the 20 flights (CASES A and B). These two flights, 11% of all liquid cloud samples, were largely responsible for the difference between the average liquid cloud properties and the average 'consistent liquid' cloud properties. These two flights were ultimately responsible for much of the difference between the drizzle and non-drizzle average properties, too. It is noteworthy that the average N_d for these two flights is roughly a factor of

560 three greater than the overall average, which is largely consistent with the ideal model of Wood (2012) and suggests that these clouds have not yet experienced drizzle. Not surprisingly the drizzling samples were, on average, found to have lower N_d and greater r_{eff} than that of the overall average. It was further concluded that much of the non-drizzling samples (after the two anomalous high N_d flights were removed) have largely similar N_d values as the drizzling liquid

565 cloud samples, suggesting that there is a possibility that these non-drizzling samples were the remains of clouds that had previously been drizzling (note that there is no direct means to infer cloud age from the limited observations). This suggestion was reached in Boers *et al.* (1996) for SOCEX I, as well.

The clouds from the two high N_d flights are unique, being the only observations of closed MCC.

570 The average results according to the MCC structure in Table 1 shows the outstanding differences in microphysical properties between the closed MCC flights and other types of MCC flights. The

link between non-drizzle and closed MCC is consistent with the observations made over the eastern Pacific during the Variability of the American Monsoon Systems Ocean-Cloud-Atmosphere-Land Study (VOCALS) experiment (Wood *et al.,* 2011). An initial, thorough

575 examination of the local and synoptic environment for these two flights failed to identify any particular forcing that may have led to the unique microphysical properties with our limited instrumentation. It is plausible that a different source of cloud condensation and/or ice nuclei could contribute to such differences, although this is speculative.

While these new observations greatly expand the climatology of SOCEX I, they are still of

580 limited scope and do not produce a full climatology of the microphysical properties of liquid water clouds over the Southern Ocean. They do, however, highlight that greater variability of N_d exists in wintertime clouds over the SO when a wider range of synoptic meteorology is investigated. They further suggest that some cloud fields are being influenced by physical processes yet to be identified. This work also serves as a basis for future research on the

585 evaluation of satellite products for effective radius and cloud droplet number concentration.

595 **Supporting information**

Figure S1. Comparisons of LWC [gm^{-3}] from different measurements.

Figure S2 Spectra by year for 2013 – 2015.

References

Ayers GP, Cainey JM. 2007. The CLAW hypothesis: a review of the major developments. *Environ Chem*, **4**(6): 366-374. doi: 10.1071/EN07080

Baumgardner D, Jonsson H, Dawson W. 2001. The cloud aerosol and precipitation spectrometer: A new instrument for cloud investigators. *Atmos. Res*. **59-6**0: 251-264. doi:10.1016/S0169-8095(01)00119-3

Bennartz R. 2007. Global assessment of marine boundary layer cloud droplet number concentration from satellite, *J. Geophys. Res.* **112**: D02201. doi: 10.1029/2006JD007547

Berg W, L'Ecuyer T, Haynes JM. 2010. The distribution of rainfall over oceans from spaceborne radars. *J. Climate*. **49**: 535–543. doi:10.1175/2009JAMC2330.1

Boers R, Jensen JB, Krummel PB, Gerber H. 1996. Microphysical and short-wave radiative structure of wintertime stratocumulus clouds over the Southern Ocean. *Quart. J. Roy. Meteor. Soc.* **122**: 1307-1339. doi: 10.1002/qj.49712253405

——,——,——. 1998. Microphysical and radiative structure of marine stratocumulus clouds over the Southern Ocean: Summer results and seasonal differences. *Quart. J. Roy. Meteor. Soc.* **124**: 151-168. doi: 10.1002/qj.49712454507

Boutle IA, Abel SJ, Hill PG, Morcrette CJ. 2014. Spatial variability of liquid cloud and rain: observations and microphysical effects. *Q. J. Roy. Meteor. Soc.* **140**: 583–594. doi:10.1002/qj.2140

Burrows SM, Hoose C, Pöschl U, Lawrence MG. 2013. Ice nuclei in marine air: Biogenic particles or dust? *Atmos. Chem. Phys.* **13**: 245-267, doi:10.5194/acp-13-245-2013.

Charlson RJ, Lovelock JE, Andreae MO, Warren SG. 1987. Oceanic phytoplankton, atmospheric sulphur, cloud albedo and climate. *Nature*. **326**: 655–661. doi: 10.1038/326655a0

Chubb TH, Siems ST, Manton MJ. 2011. On the decline of wintertime precipitation in the Snowy Mountains of southeastern Australia. *Journal of Hydrometeorology*. **12** (6): 1483-1497. doi: 10.1175/JHM-D-10-05021.1

——, Jensen JB, Siems ST, Manton MJ. 2013. In situ observations of supercooled liquid clouds over the Southern Ocean during the HIAPER Pole-to-Pole Observation campaigns. *Geophys. Res. Lett*. **40**: 5280–5285. doi:10.1002/grl.50986

——, Huang Y, Jensen JB, Campos T, Siems ST, Manton MJ. 2016. Observations of high droplet number concentrations in Southern Ocean boundary layer clouds. *Atmospheric Chemistry and Physics [P]*. **16** (2) : 971-987. doi: 10.5194/acp-16-971-2016

Cober SG, Isaac GA, Korolev AV. 2000. 'Assessing the relative contribution of liquid and ice phases in winter clouds'. Pp. 689–693 in *Proceedings of 13th International Conference on clouds and precipitation*, 14–18 August, 2000, Reno, Nevada, USA. doi: http://dx.doi.org/10.1175/1520-0450(2001)040<1967:ACPC>2.0.CO;2

——, ——, ——, Strapp JW. 2001. Assessing cloud-phase conditions. *J. Appl. Meteorol*. **40**: 1967–1983. doi: http://dx.doi.org/10.1175/1520-0450(2001)040<1967:ACPC>2.0.CO;2

Dong X, Mace GG. 2003. Arctic Stratus Cloud Properties and Radiative Forcing Derived from Ground-Based Data Collected at Barrow, Alaska. *J. Clim*. **16**: 445–461. doi: http://dx.doi.org/10.1175/1520-0442(2003)016<0445:ASCPAR>2.0.CO;2

Draxler R, Hess G. 1998. An overview of the HYSPLIT_4 modelling system for trajectories, dispersion and deposition. *Aust. Meteorol. Mag*. **47**: 295–308

Ellis TD, L'Ecuyer T, Haynes JM, Stephens GL. 2009. How often does it rain over the global oceans? The perspective from CloudSat. *Geophys. Res. Lett*. **36**: L03815. doi:10.1029/2008GL036728

Gras JL. 1995. CN, CCN and particle size in southern ocean air at cape grim. *Atmos. Res*. **35**:

645 233–251. doi:10.1016/0169-8095(94)00021-5

Gultepe I, Isaac GA. 2002. The effects of air-mass origin on Arctic cloud microphysical parameters for April 1998 during FIRE.ACE. *J. Geophys. Res*. **107**(10) SHE 4–1 to 4–12. doi: 10.1029/2000JC000440

Han QY, Rossow WB, Chou J. 1998. Global survey of the relationships of cloud albedo and

650 liquid water path with droplet size using ISCCP. *J. Clim*. **11**: 1516-1528. doi:10.1175/1520-0442(1998)011<1516:GSOTRO>2.0.CO;2

Mossop SC, Ono A, Wishart ER. 1970. Ice particles in maritime clouds near Tasmania. *Quart. J. Roy. Meteor. Soc*. **96**: 487–508. doi:10.1002/qj.49709640910

Hoskins BJ, Hodges KI. 2005. A New Perspective on Southern Hemisphere Storm Tracks.

655 *Journal of Climate*. **18**(20): 4108-4109,4111-4113,4115-4116,4118-4129. doi: http://dx.doi.org/10.1175/JCLI3570.1

Hu Y, Rodier S, Xu K. 2010. Occurrence, liquid water content, and fraction of supercooled water clouds from combined CALIOP/IIR/MODIS measurements. *J. Geophys. Res*. **115**: D00H34. doi:10.1029/2009JD012384

660 Huang Y, Siems ST, Manton MJ, Protat A, Delanoë J. 2012a. A study on the low-altitude clouds over the Southern Ocean using the DARDAR-MASK. *J. Geophys. Res*. **117**: D18204. doi:10.1029/2012JD017800

——, ——, ——, Hande LB, Haynes J M. 2012b. The structure of low-altitude clouds over the Southern Ocean as seen by CloudSat. *J. Climate*. **25**: 2535–2546. doi:10.1029/2012JD017800

665 ——, ——, ——, Thompson G. 2014. An evaluation of WRF simulations of clouds over the Southern Ocean with A-Train observations. *Mon. Weather Rev*. **142**: 647–667. doi: 10.1175/MWR-D-13-00128.1

——, Franklin CN, Siems ST, Manton MJ, Chubb TH, Lock A, Alexander S, Klekociuk A. 2015a. Evaluation of boundary-layer cloud forecasts over the Southern Ocean in a limited-area numerical weather prediction system using in situ, space-borne and ground-based observations. *Q. J. Roy. Meteor. Soc*. **141**: 2259–2276. doi:10.1002/qj.2519

——, Protat A, Siems ST, Manton MJ. 2015b. A-Train observations of maritime mid latitude storm-track cloud systems: comparing the Southern Ocean against the North Atlantic. *Journal Of Climate* [P]. **28**(5): 1920-1939. doi:10.1175/JCLI-D-14-00169.1

Isaac GA, Cober SG, Strapp JW, Korolev AV, Tremblay A, Marcotte DL. 2001. Recent Canadian research on aircraft in-flight icing. *Can. Aeronaut. Space J*. **47**: 213–221

Korolev, AV. 2007. Reconstruction of the Sizes of Spherical Particles from Their Shadow Images. Part I: Theoretical considerations. J. Atmos. Oceanic Technol., 24, 376–389, doi: http://dx.doi.org/10.1175/JTECH1980.1

——, Isaac GA. 1998. 'Phase composition of stratiform clouds'. Pp. 129–146 in *Proceedings of FAAWorkshop on mixed-phase and glaciated icing conditions*, *2 & 3 Dec. 1998*. Federal Aviation Authority, Atlantic City, NJ, USA.

——, ——. 2000. 'Phase composition of stratiform clouds'. Pp. 725–727 in *Proceedings of 13th Int. Conf. on clouds and precipitation*, *14–18 August, 2000*. Reno, Nevada, USA.

——, ——, Cober SG, Strapp JW, Hallett J. 2003. Microphysical characterization of mixed-phase clouds. Q. J. R. Meteorol. Soc. **129**: 39– 65

——, Emery EF, Strapp JW, Cober SG, Isaac GA. 2013. Quantification of the effects of shattering on airborne ice particle measurements. *J. Atmos. Oceanic Technol*. **30**(11): 2527–2553. doi:10.1175/JTECH-D-13-00115.1

Lilie L, Emery E, Strapp J, Emery J. 2005. 'A Multiwire Hot-Wire Device for Measurement of Icing Severity, Total Water Content, Liquid Water Content, and Droplet Diameter'. *43rd AIAA*

Aerospace Sciences Meeting and Exhibit. Aerospace Sciences Meetings.

Mace GG, Marchand R, Zhang Q. 2007. Global hydrometeor occurrence as observed by CloudSat: Initial observations from summer 2006. *Geophys. Res. Lett.* **34**: L09808. doi: 10.1029/2006GL029017

Mazin IP, Nevzorov AN, Shugaev VP, Korolev AV. 1992. 'Phase structure of stratiform clouds'. Pp. 332–336 in *Proceedings of 11th Int. Conf. on clouds and precipitation*, *17–21 August, 1992*, Montreal, Canada.

McCoy DT, Hartmann DL, Grosvenor DP. 2014. Observed Southern Ocean cloud properties and shortwave reflection. Part II: Phase changes and low cloud feedback. *J. Climate.* **27***:* 8858–8868. doi: http://dx.doi.org/10.1175/JCLI-D-14-00288.1

——, Burrows SM, Wood R, Grosvenor DP, Elliott SM, Ma P, Rasch PJ, Hartmann DL. 2015. Natural aerosols explain seasonal and spatial patterns of Southern Ocean cloud albedo. *Sci. Adv.* **1**(6): e1500157. doi: 10.1126/sciadv.1500157

McFarquhar, Greg M., Junshik Um, and Robert Jackson. (2013), Small Cloud Particle Shapes in Mixed-Phase Clouds, *Atmospheric Research* **180**, 226-240.

Morrison, A.E., S.T. Siems, M.J. Manton, A. Nazarov, 2010: A Modelling Case Study of Mixed Phase Clouds over the Southern Ocean and Tasmania. *Monthly Wea. Rev.,* **138**, 839-862, doi: 10.1175/2009MWR3011.1.

——, ——, ——. 2011. A Three-Year Climatology of Cloud-Top Phase over the Southern Ocean and North Pacific. *J. Clim.* **24**: 2405-2418. doi:10.1175/2010JCLI3842.1

——, ——, ——. 2013. On a natural environment for glaciogenic cloud seeding, *Journal of Applied Meteorology and Climatology.* **52**(5): 1097(8). doi: http://dx.doi.org/10.1175/JAMC-D-12-0108.1

715   Muhlbauer A, McCoy IL, Wood R. 2014. Climatology of stratocumulus cloud morphologies: microphysical properties and radiative effects. *Atmos. Chem. Phys.* **14**: 6695–6716. doi:10.5194/acp-14-6695-2014

Pruppacher HR, Klett JD. 2010. *Microphysics of Clouds and Precipitation*. Springer Netherlands; ch 10. pp 361-444 doi: 10.1007/978-0-306-48100-0

720   Quinn P, Bates T. 2011. The case against climate regulation via oceanic phytoplankton sulphur emissions. *Nature.* **480**: 51–56. doi:10.1038/nature10580

Risbey JS, Pook MJ, Mclntosh PC, Ummenhofer CC, Meyers G. 2009. Characteristics and variability of synoptic features associated with cool season rainfall in southeastern Australia. Int. *J. Climatol.* **29**: 1595–1613. doi: 10.1002/joc.1775

725   Daniel Rosenfeld, Hailong Wang, Philip J. Rasch. 2012, The roles of cloud drop effective radius and LWP in determining rain properties in marine stratocumulus, *Geophys. Res. Lett.*, **39**: L13801, doi:10.1029/2012GL052028.

Simmonds I, Keay K. 2000. Mean Southern Hemisphere extratropical cyclone behavior in the 40-Year NCEP–NCAR Reanalysis. *J. Clim.* **13**: 873–885. doi:10.1175/ 1520-

730   0442(2000)013,0873:MSHECB.2.0.CO;2

Trenberth KE, Fasullo JT. 2010. Simulation of Present-Day and Twenty-First-Century Energy Budgets of the Southern Oceans. *J. Climate.* **23**: 440-454. doi:101175/2009JCLI3152.1

Wang Z, Siems ST, Belusi, D, Manton MJ, Huang, Y. 2015. A climatology of the precipitation over the Southern Ocean as observed at Macquarie Island. *Journal of Applied Meteorology and*

735   *Climatology* [P]. **54**(12): 2321-2337. doi: 10.1175/JAMC-D-14-0211.1

Wofsy S. 2011. HIAPER Pole-to-Pole Observations (HIPPO): fine-grained, global-scale measurements of climatically important atmospheric gases and aerosols. *Philos. T. R. Soc. A.* **369**: 2073–2086. doi: 10.1098/rsta.2010.0313

Wood R. 2012. Stratocumulus clouds, *Mon. Wea. Rev.* **140**: 2373-2423. doi:

740   http://dx.doi.org/10.1175/MWR-D-11-00121.1

——, Bretherton C, Leon D, Clarke A, Zuidema P, Allen G, Coe H. 2011. An aircraft case study

of the spatial transition from closed to open mesoscale cellular convection over the southeast

Pacific. *Atmos. Chem. Phys*. **11**: 2341–2370. doi:10.5194/acp-11-2341-2011

——, Leon D, Lebsock M, Snider J, Clarke AD. 2012. Precipitation driving of droplet

745   concentration variability in marine low clouds. *J. Geophys. Res*. **117**: D19210.

doi:10.1029/2012JD018305

——, Hartmann DL. 2006. Spatial variability of liquid water path in marine boundary layer

clouds: The importance of mesoscale cellular convection. *J. Climate*. **19**: 1748–1764. doi:

http://dx.doi.org/10.1175/JCLI3702.1

750   ——, Field PR. 2011. The distribution of cloud horizontal sizes. *J. Clim.* **24**: 4800–4816.

doi: 10.1175/2011JCLI4056.1

Figure Captions

755   Figure 1. 72-hour Hybrid Single Particle Lagrangian Integrated Trajectory Model (HYSPLIT) back trajectories for 20 flights of three consecutive winters (Jun - Oct, 2013 - 2015) with the Global Data Assimilation System (GDAS) reanalysis. Left panel is for research flights and right panel is for operational (seeding) flights. The flights dates are indicated with the alphabets on the trajectory line. The calculation of each back trajectory was initialised for the average altitude of

760   the samples for the flight. ~~Each trajectory ran on its average height showing consistency during the flight with different heights.~~ The colouring of each back trajectory changes for each 24-hour period. The two non-drizzling cases (CASES A and B) are indicated by a reddish colour with big circle marks, while the two heavily drizzling cases (CASES C and D) are indicated by a reddish colour with star marks.

765   Figure 2. Fractions of cloud phase coefficient (μ3) for different temperature intervals for 20 flights of three consecutive winters (Jun - Oct, 2013 - 2015).

        Figure 3. Averaged microphysical properties and spectra by temperature for liquid clouds from 20 flights observations of three consecutive winters (Jun - Oct, 2013 - 2015). (a) Fraction by temperature, (b) r_{eff} and N_d by temperature, (c) LWC by temperature, (d) cloud number

770   concentration spectra by temperature, and (e) LWC spectra by temperature. (a) and (b) The horizontal error bars are standard deviations.

        Figure 4. The probability density function (PDF) of N_d (a), r_{eff} (CAS + CIP) (b), LWC (CAS+CIP) (c), and the spectra (d) of drizzling and non-drizzling liquid clouds from 20 flights observations of three consecutive winters (Jun - Oct, 2013 - 2015).

775   Figure 5. The probability density function (PDF) of drizzling and non-drizzling sections of liquid

clouds from 20 flights observations of three consecutive winters (Jun - Oct, 2013 - 2015). The

cloud distributions are analysed by consistent drizzle or non-drizzle cloud sections for each time

period (e.g. 21-30 seconds).

Figure 6. Comparison of r_{eff} and spectra for CASES A and B against all 18 flights. 'All' means

780   all flights except CASES A and B. (a) Mean r_{eff} and r_{effT} (CAS+CIP) by pressure. The r_{effT}

(CAS+CIP) at the 1000 - 950 hPa is written on the plot as 69. The horizontal error bars on r_{eff} are

standard deviations. The standard deviations of r_{effT} (CAS+CIP) are indicated in the parenthesis

(b) Particle size spectra of all flights and CASES A and B.

Figure 7. MODIS satellite images (a) ~ (d) and soundings (e) ~ (h) for two minimum drizzle

785   cases, CASES A and B (23 Jul 2013 and 01 Oct 2015, respectively) and two heavily drizzle

cases, CASES C and D (28 Jun 2013 and 30 Aug 2015, respectively). (a) ~ (d) The locations

where each flight was flown are indicated with red circle. The times of the images taken are 1425,

1425, 1430, and 1425 AEST, respectively. (e) ~ (h) The times when the soundings made are

about 1600, 1313, 1335, and 1342 AEST respectively.

790   Figure 8. Vertical profile of cloud microphysical properties (Nd, reff, and LWC) from the

soundings of non-drizzling cases (CASES A and B) and drizzling dominant (CASES C and D)

flights in Figure 7(e) ~ (h). The estimated cloud base and top heights are indicated by the dashed

lines. The error bars are standard deviations.

795

Table Captions

Table 1. Summary of synoptic conditions and average thermodynamic and cloud microphysical properties for each flight for winter time during 2013 - 2015. Microphysical properties categorised by 'Research/Operational (Seeding)' flights and the types of MCC are also

800   summarised at the bottom of the table. The MCC categorization is not determined for a flight (20140630) due to its ambiguous morphological image. The thermodynamic and microphysical properties are averaged by 1 second sampling.

Table 2. Overall averages of the liquid-only cloud average microphysical properties for 20 flights observations of three consecutive winters (Jun - Oct, 2013 - 2015). 'Boers method' is average of

805   representative averages (Table 1) of all flights. 'Simple average' is average of all cloud samples from all flights. 'Consistent liquid average' is average for consistent liquid clouds which are consistent over a minimum time period of 5 minutes (~ 30 km). The numbers in parenthesis are standard deviations (s.d.).

Table 3. Summary of microphysical properties of 1 second and 10 seconds consistent drizzle and

810   non-drizzle sections of clouds from 20 flights observations of three consecutive winters (Jun - Oct, 2013 - 2015). The standard deviations (s.d.) are indicated in the parenthesis.

Table 4. Comparison of thermodynamic and microphysical properties and meteorology from the soundings for two non-drizzle dominant cases (CASES A and B, 23 July 2013 and 01 October 2015, respectively) and two drizzle dominant cases (CASES C and D, 28 June 2013 and 30

815   August 2015, respectively). [1] MCC (mesoscale cellular convection). [2] The interpretation of the

MODIS image displays a hardship to clear identify with the presence of multi-level clouds. The standard deviations (s.d.) are indicated in the parenthesis for the cloud microphysical properties.

Flight Locations and Air mass Back Trajectories

(a) 20130815_1224	(e) 20130707_1259	(i) 20130723_1302
(b) 20131011_1324	(f) 20130806_1513	(j) 20151001_1230
(c) 20140912_1243	(g) 20130907_1224	(k) 20130628_1301
(d) 20140903_1243	(h) 20130614_1336	(l) 20150830_1305

(m) 20130921_1133	(q) 20140806_1508
(n) 20131011_0749	(r) 20150804_1219
(o) 20130803_0844	(s) 20130707_0737
(p) 20130702_1011	(t) 20140630_0708
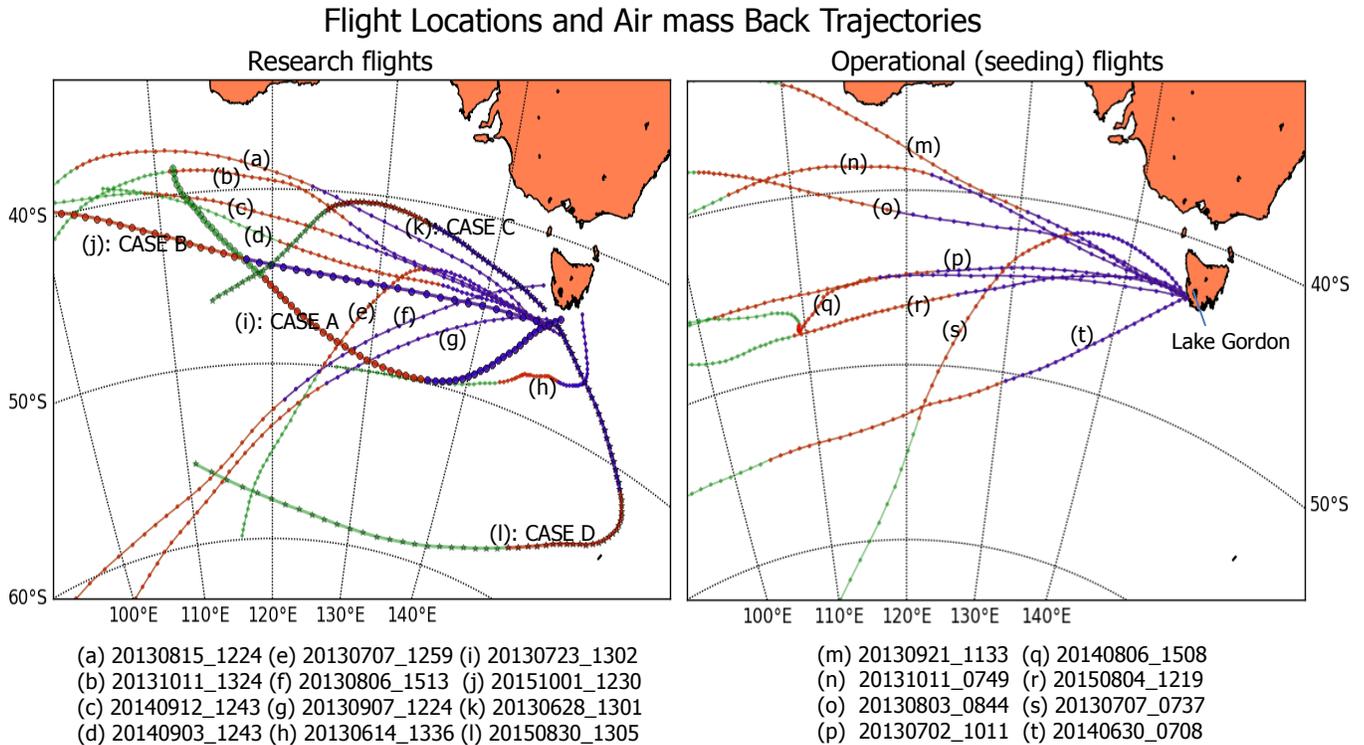
Figure 1. Seventy-two hour Hybrid Single Particle Lagrangian Integrated Trajectory Model (HYSPLIT) back trajectories for 20 flights of three consecutive winters (Jun - Oct, 2013 - 2015) with the Global Data Assimilation System (GDAS) reanalysis. The left panel is for research flights and the right for operational (seeding) flights. The flights dates are indicated by the letter on the trajectory line. The calculation of each back trajectory was initialised for the average altitude of the samples for the flight. ~~Each trajectory ran on its average height showing consistency during the flight with different heights.~~ The colouring of each back trajectory changes for each 24h period. The two non-drizzling cases (CASES A and B) are indicated by a

reddish colour with big circle marks, while the two heavily drizzling cases (CASES C and D) are

indicated by a reddish colour with star marks.

830
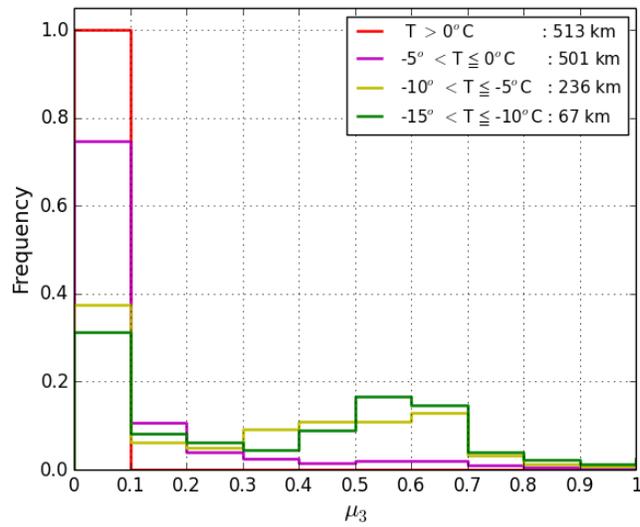
Figure 2. Fractions of cloud phase coefficient (μ_3) for different temperature intervals for 20 flights of three consecutive winters (Jun - Oct, 2013 - 2015).
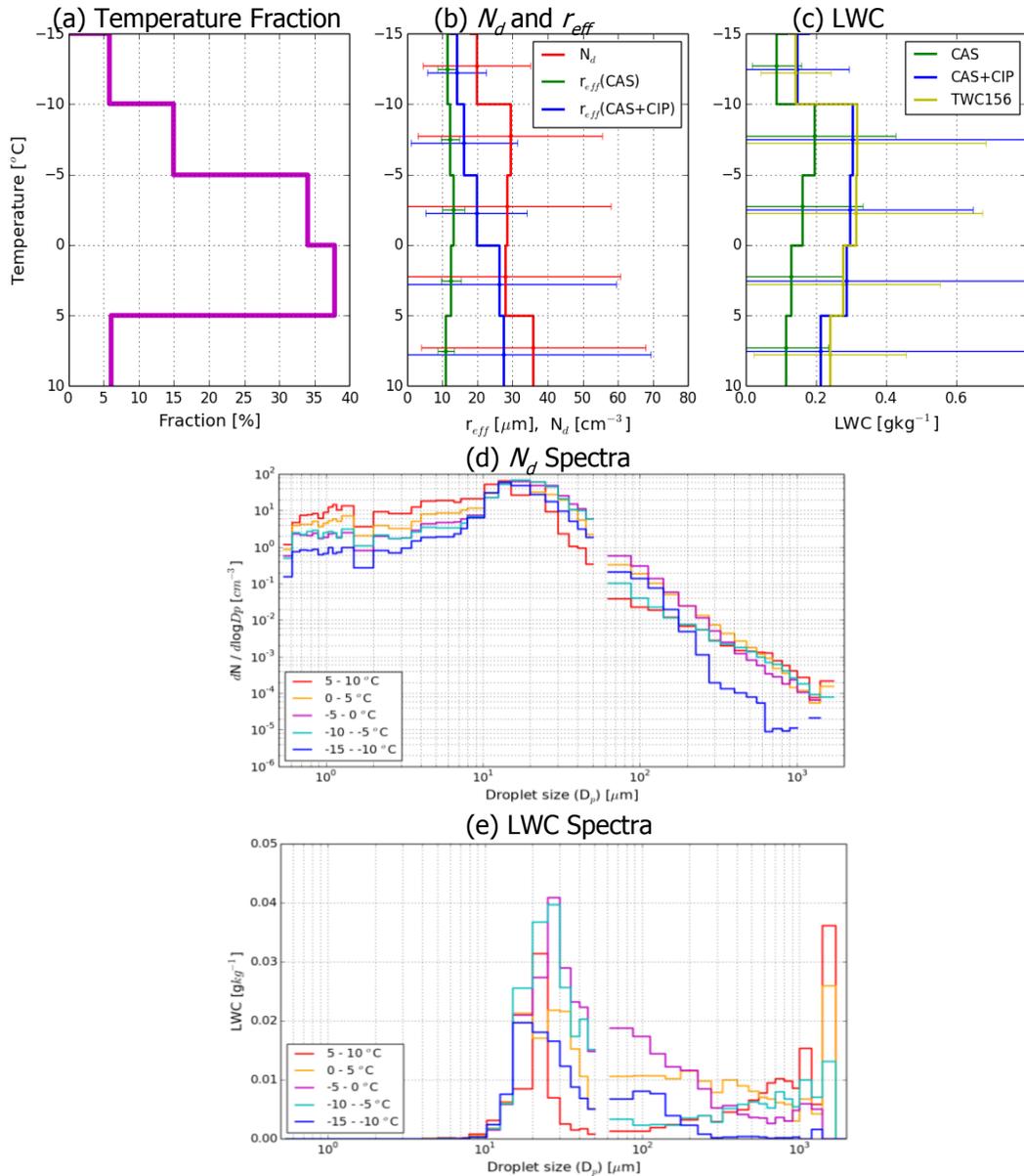
Figure 3 Averaged microphysical properties and spectra by temperature for liquid clouds from 20 flights' observations of three consecutive winters (Jun - Oct, 2013 - 2015). (a) Fraction by temperature, (b) r_{eff} and N_d by temperature, (c) LWC by temperature, (d) cloud number concentration spectra by temperature, and (e) LWC spectra by temperature. In (b) and (c), The horizontal error bars are standard deviations.
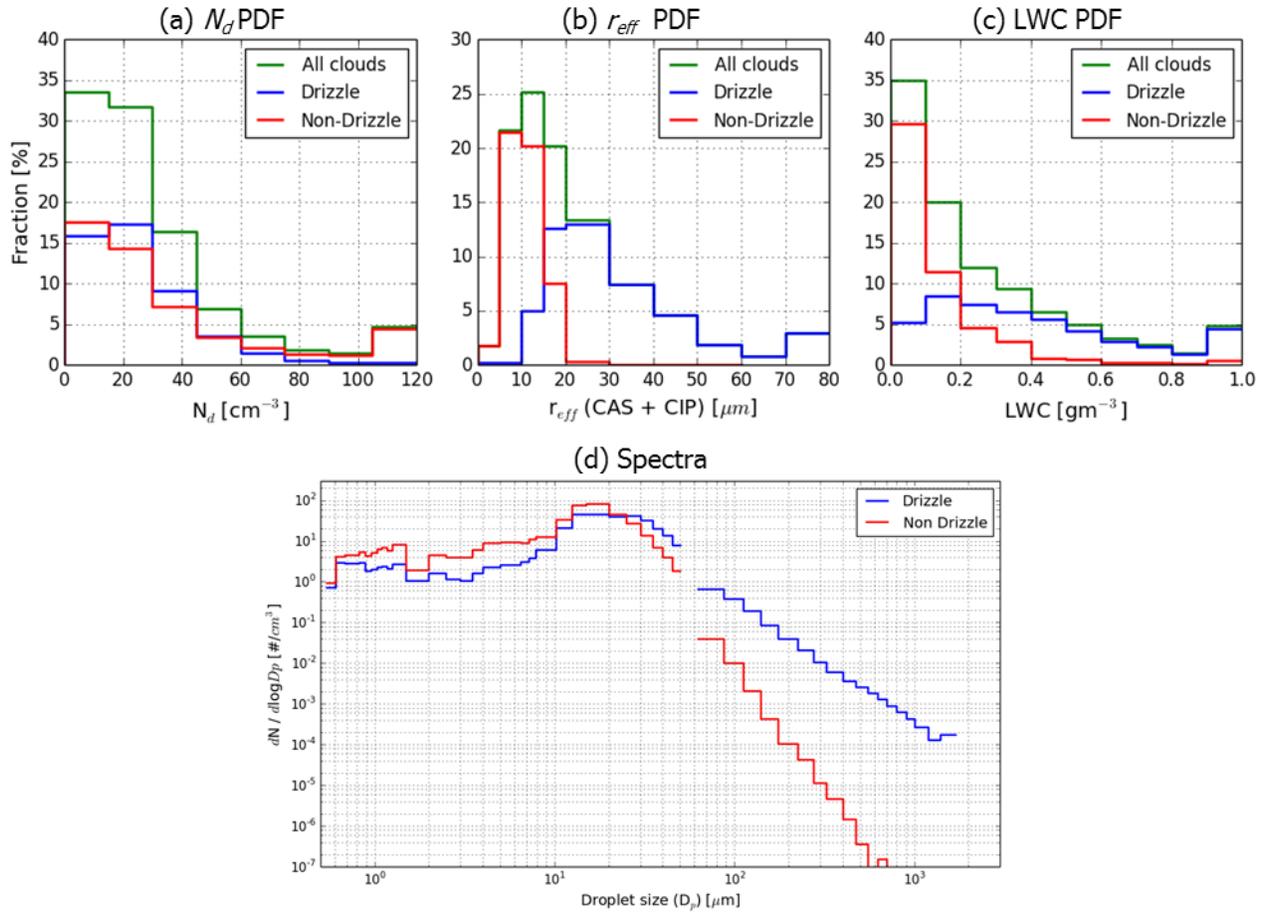
Figure 4. The probability density function (PDF) of (a) N_d, (b) r_{eff} (CAS + CIP), (c) LWC (CAS+CIP), and (d) the spectra of drizzling and non-drizzling liquid clouds from 20 flights' observations of three consecutive winters (Jun - Oct, 2013 - 2015).
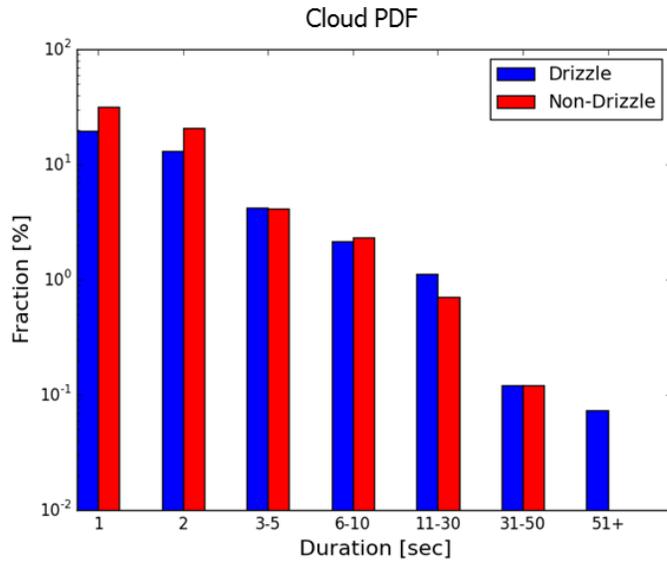
845 Figure 5. The probability density function (PDF) of drizzling and non-drizzling sections of liquid clouds from 20 flights observations of three consecutive winters (Jun - Oct, 2013 - 2015). The cloud distributions are analysed by consistent drizzle or non-drizzle cloud sections for each time period (e.g. 11-30 s).
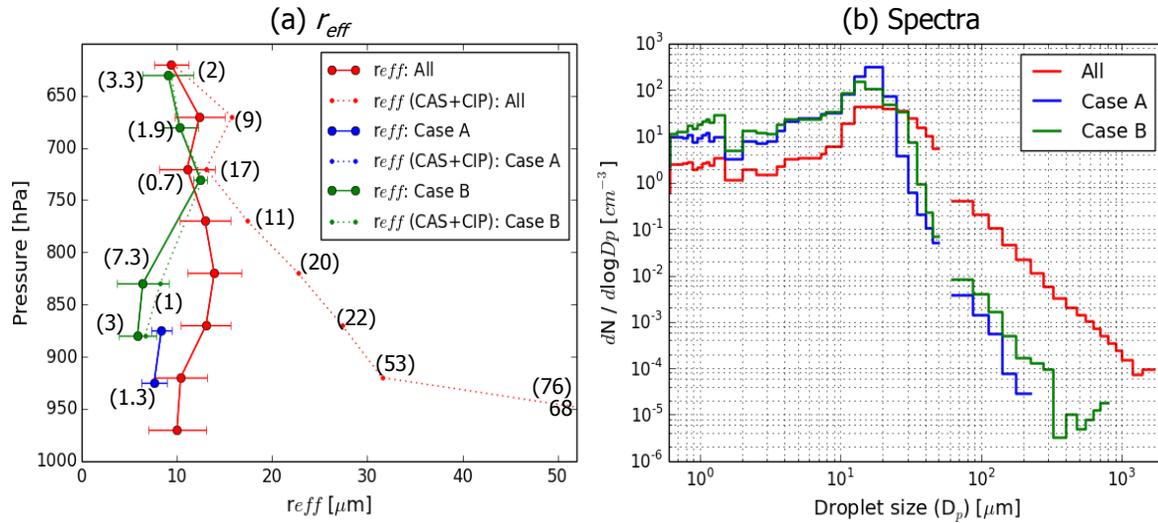
Figure 6. Comparison of r_{eff} and spectra for CASES A and B against all 18 flights. 'All' means all flights except CASES A and B. (a) Mean r_{eff} and r_{effT} (CAS+CIP) by pressure. The r_{effT} (CAS+CIP) at the 1000 to 950 hPa is written on the plot as 68. The horizontal error bars on r_{eff} are standard deviations. The standard deviations of r_{effT} (CAS+CIP) are indicated in the parentheses (b) Particle size spectra of all flights and CASES A and B.
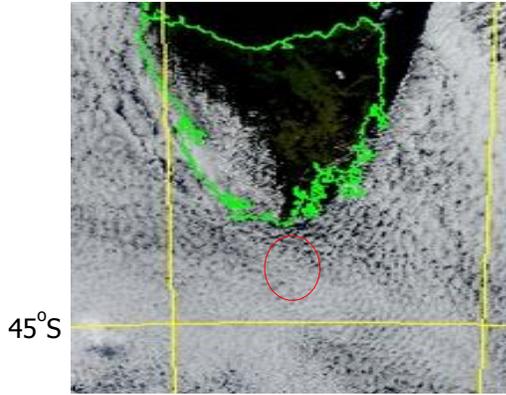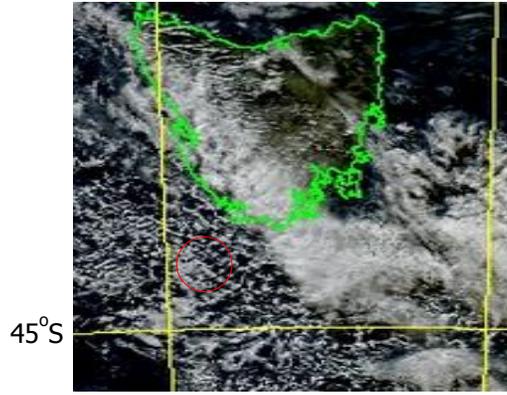
(a) CASE A

(c) CASE C

(b) CASE B
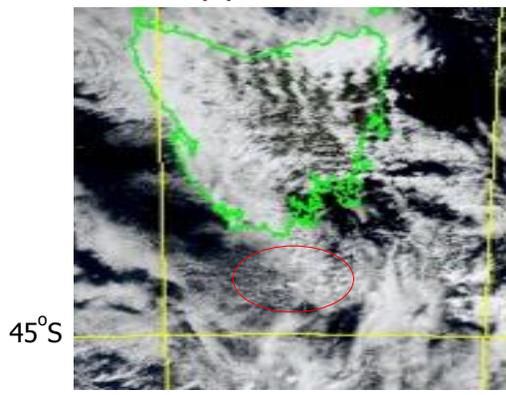
(d) CASE D
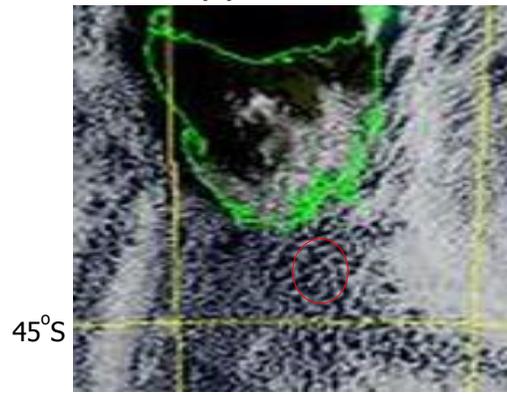
(e) CASE A
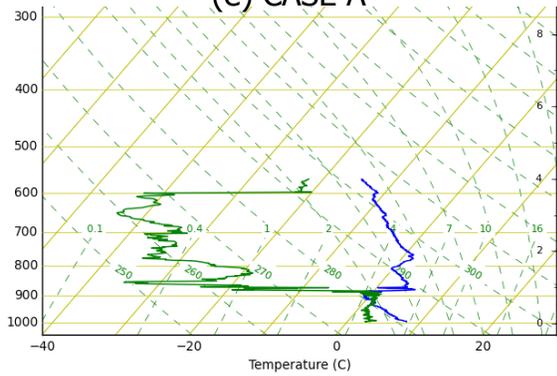
(g) CASE C
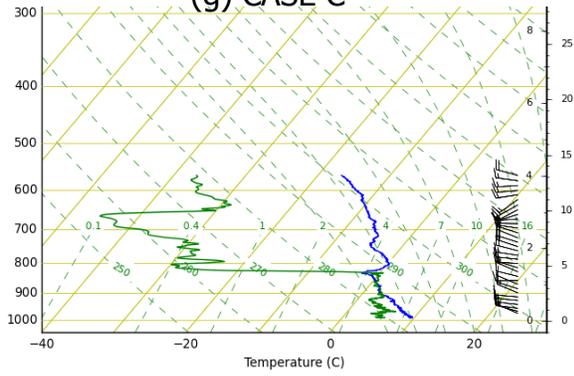
(f) CASE B
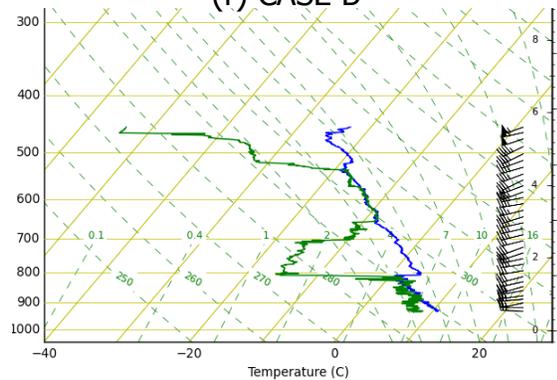
(h) CASE D
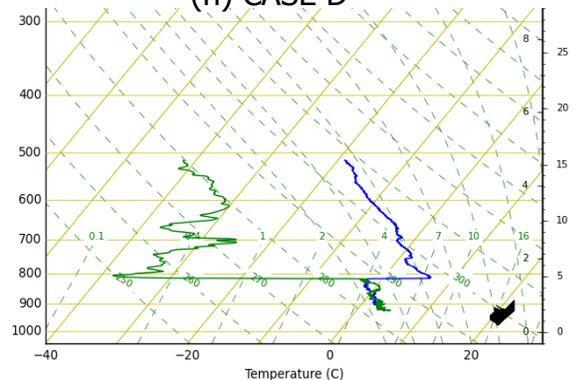
Figure 7. MODIS satellite images (a) - (d) and soundings (e) - (h) for two minimum drizzle cases, CASES A and B (23 July 2013 and 01 October 2015, respectively) and two heavily drizzle cases, CASES C and D (28 June 2013 and 30 August 2015, respectively). (a) - (d) The locations where each flight was flown are indicated with a red circle. The times of the images taken are 1425, 1425, 1430, and 1425 AEST (UTC + 10h), respectively. (e) - (h) The times when the soundings made are about 1600, 1313, 1335, and 1342 AEST respectively.

860
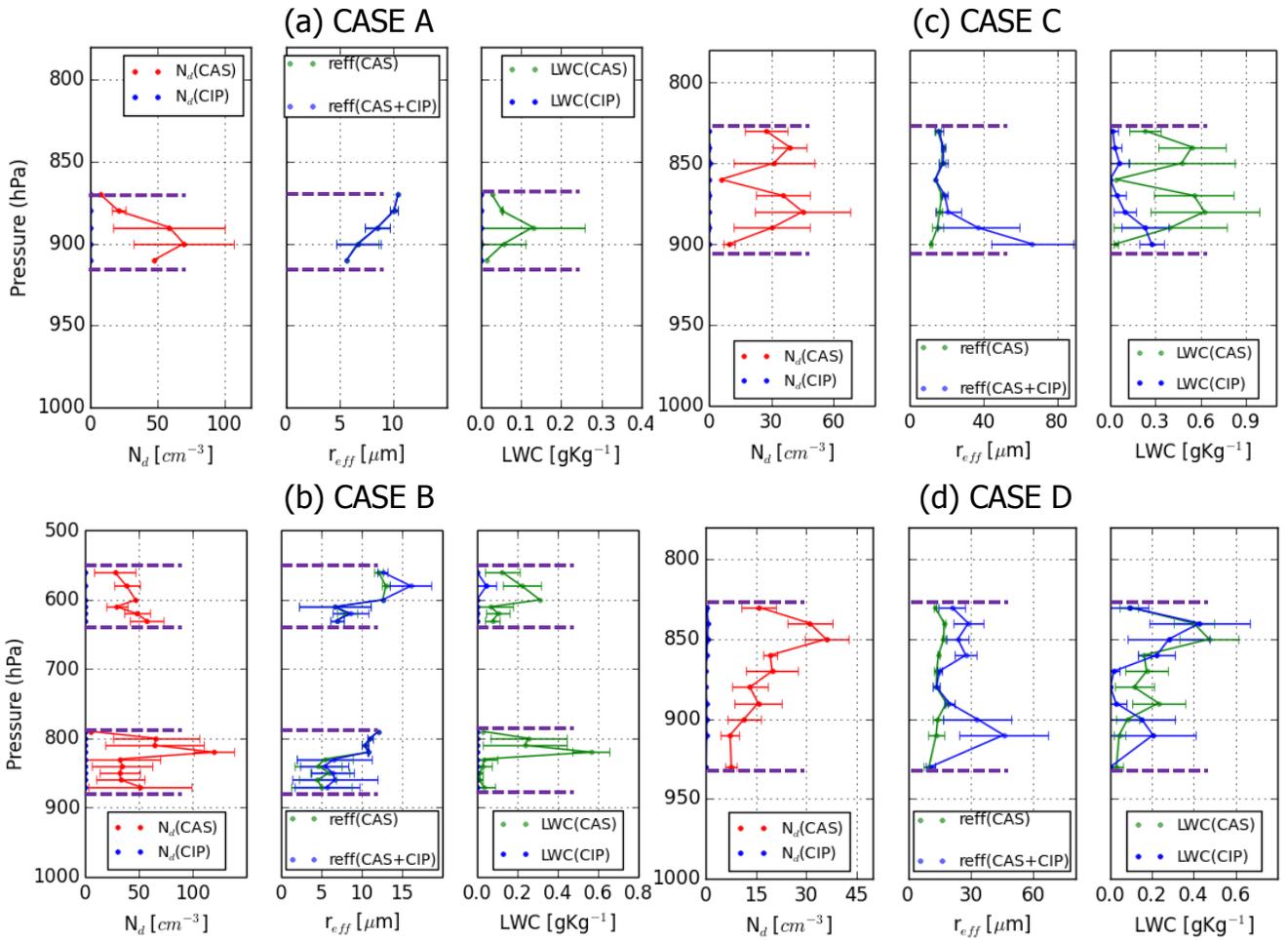
Figure 8. (a) – (d) Vertical profile of cloud microphysical properties (N_d, r_{eff}, and LWC) from the soundings of non-drizzling cases (CASES A and B) and drizzling dominant (CASES C and D) flights in Figure 7(e) ~ (h). The estimated cloud base and top heights are indicated by the dashed lines. The error bars are standard deviations.

Summary of synoptic conditions and thermodynamic and cloud microphysical properties for each flight

870

Flight Date/ Category	Type[1]	Flight Location	Front association[2]	Cloud Type[3]	Pressure [hPa]	Cloud Base[4] [km]	Cloud Top[4] [km]	Wind Direction [°]	Time in Clouds [sec]	Liq Fraction [%]	Mxd Fraction [%]	Ice Fraction [%]	Temperature [°C]	N_d [cm^{-3}]	r_{eff} [μm]	r_{eff} (CAS+CIP) [μm]	LWC(CAS) [gkg^{-1}]	LWC (CAS+CIP) [gkg^{-1}]	Drizzle [%]	RainRate [mmhr^{-1}]
20130803_084439	O[5]	SW	Prefrontal	No MCC	683	2.5	3.8	261	541	19%	79.1%	1.7%	-10.8 (-11.2 ~ -10.3)	7	12.3	31.5	0.034	0.234	89%	0.328
20130707_125944	R	S	Prefrontal	Open MCC	915	0.5	1.0	274	2022	10%	89.6%	0.7%	-0.1 (-9.3 ~ 4.0)	11	13.7	56.3	0.093	0.305	59%	3.667
20150830_130524	R	S	Not associated	Open MCC	867	0.7	1.5	151	1754	98%	1.6%	0.0%	0.5 (-4.7 ~ 4.2)	13	13.2	35.9	0.079	0.390	91%	0.957
20131011_074911	O	W	Near front (~50km)	No MCC	853	0.7	1.5	276	266	91%	3.8%	5.6%	2.1 (-0.8 ~ 7.6)	13	13.6	16.9	0.076	0.112	60%	0.112
20130707_073753	O[5]	W	Prefrontal	Open MCC	766	1.6	2.3	320	377	32%	50.4%	17.2%	-10.3 (-13.2 ~ 6.7)	15	15.4	20.6	0.155	0.234	49%	0.363
20140630_070840	O	W	Prefrontal	Not identified	693	N/A	N/A	259	899	50%	46.8%	3.1%	-9.5 (-10.3 ~ -8.4)	15	13.4	14.2	0.105	0.120	5%	0.046
20150804_121910	O	W	Prefrontal	Open MCC	667	N/A	N/A	279	496	14%	80.2%	5.6%	-11.0 (-12.0 ~ -9.6)	17	14.0	15.8	0.140	0.184	27%	0.267
20130815_122404	R	SW	Ridge	Disorganized MCC	778	0.9	2.0	302	1380	65%	35.1%	0.0%	-4.5 (-6.9 ~ 5.6)	18	11.2	11.3	0.072	0.076	10%	0.007
20130702_101141	O	W	Near front (~120km)	No MCC	853	1.0	2.1	275	1728	35%	55.3%	9.9%	0.1 (-7.3 ~ 4.9)	19	14.2	45.6	0.137	0.422	83%	3.250
20140903_124321	R	S,SW	Ridge	Open MCC	801	1.2	2.0	224	694	70%	29.3%	0.7%	-2.3 (-9.2 ~ 7.4)	21	14.0	19.0	0.173	0.231	37%	0.412
20130628_130139	R	SW	Ridge	Open MCC	871	0.7	1.6	194	1338	93%	6.7%	0.0%	-0.6 (-4.5 ~ 8.0)	21	14.2	23.3	0.190	0.306	85%	0.441
20140912_124317	R	S	Not associated	Open MCC	809	1.4	1.9	264	1433	69%	29.2%	1.4%	-1.2 (-11.4 ~ 5.0)	21	14.0	18.8	0.195	0.388	47%	3.160
20130614_133658	R	SE	Not associated	Open MCC	882	1.0	1.4	145	1201	99%	1.4%	0.0%	0.0 (-5.2 ~ 2.6)	23	13.1	20.3	0.159	0.275	62%	1.002
20140806_150804	O	W	Near front (~50km)	No MCC	666	2.0	3.3	264	556	9%	90.8%	0.0%	-8.6 (-9.4 ~ -7.8)	28	12.1	15.2	0.169	0.217	34%	0.496
20130921_113331	O	W	Near front (~400km)	No MCC	656	2.2	2.5	257	189	88%	12.2%	0.0%	-8.4 (-10.1 ~ -2.1)	28	9.8	9.5	0.101	0.101	0%	0.0
20131011_132432	R	S	Postfrontal	Disorganized MCC	804	0.7	2.4	273	1904	82%	16.6%	0.9%	-1.3 (-25.2 ~ 8.4)	29	11.2	21.3	0.130	0.219	44%	1.112
20130907_122442	R	SW	Postfrontal	Open MCC	804	0.6	1.9	257	1742	49%	51.0%	0.0%	-6.4 (-10.9 ~ 5.8)	34	13.2	24.0	0.257	0.422	58%	1.788
20130806_151347	R	W	Postfrontal	Open MCC	810	1.0	2.5	249	355	95%	5.4%	0.0%	-6.0 (-13.6 ~ -2.7)	40	11.3	12.2	0.201	0.202	0%	0.0
20151001_123025	R	S	Postfrontal	Closed MCC	779	1 3.4	1.8 4.3	260	803	68%	32.0%	0.2%	-1.6 (-18.7 ~ 9.1)	80	8.5	8.5	0.172	0.173	4%	0.007
20130723_130219	R	S	Ridge	Stratiforn closed MCC	904	0.8	1.2	183	679	100%	0.0%	0.0%	-0.1 (-3.2 ~ 4.0)	89	8.2	8.2	0.165	0.165	0%	0.0
Research Flights			-						15305	70%	29.6%	0.4%		33	12	22	0.157	0.263	51%	1.046
Operational Flights			-						5052	36%	58.0%	6.3%		18	13	21	0.114	0.203	47%	0.608
Closed MCC			-						1482	83%	17.3%	0.1%		84	8	8	0.169	0.169	2%	0.004
Open MCC			-						11412	63%	35.6%	1.2%		21	14	25	0.164	0.294	65%	1.206
Disorganised MCC			-						3284	75%	24.4%	0.5%		23	11	16	0.101	0.148	31%	0.559
No MCC			-						3280	35%	58.6%	5.9%		19	12	24	0.103	0.217	65%	0.837
Total (mean)									20,357	61.5%	36.7%	1.8%		27	12.5	21.4	0.140	0.239	49%	0.733

[1] Flight type: R (Research), O (Operational) [2] Approximate distance from the front is indicated in the parenthesis [3] Cloud type: MCC (Mesoscale cellular convection) [4] Approximate bounds from soundings, when available. Note that the cloud fields were not horizontally homogeneous, and multiple layers commonly were observed [5] No seeding activities were conducted

Table 1. Summary of synoptic conditions and average thermodynamic and cloud microphysical

875   properties for each flight for winter time during 2013 - 2015. Microphysical properties

categorised by 'Research/Operational (Seeding)' flights and the types of MCC are also

summarised at the bottom of the table. The MCC categorization is not determined for a flight

(20140630) due to its ambiguous morphological image. The thermodynamic and microphysical

properties are averaged by 1 second sampling.

880

Different method/source of average	N_d [cm^{-3}] (s.d.)	r_{eff} [μm] (s.d.)	LWC [gkg^{-1}] (s.d.)
Boers method (CAS only)	27 (21)	12.6 (2.0)	0.140 (0.054)
Boers method (CAS + CIP)	27 (21)	21.4 (12.5)	0.239 (0.103)
Simple average (CAS only)	28 (30)	12.5 (2.9)	0.146 (0.167)
Simple average (CAS + CIP)	28 (30)	21.6 (25.7)	0.268 (0.897)
Consistent liquid average (CAS only)	40 (41)	11.4 (3.0)	0.122 (0.122)
Consistent liquid average (CAS +CIP)	40 (41)	22.4 (28.2)	0.227 (0.494)
SOCEX I average (FSSP only)	28 (11)	12.4 (1.8)	0.129 (0.03)

Table 2. Overall averages of the liquid-only cloud average microphysical properties for 20 flights' observations of three consecutive winters (Jun - Oct, 2013 - 2015). 'Boers method' is average of representative averages (Table 1) of all flights. 'Simple average' is average of all cloud samples from all flights. 'Consistent liquid average' is average for consistent liquid clouds which are consistent over a minimum time period of 5 minutes (~ 30 km). The numbers in parentheses are standard deviations (s.d.).

885

6

Cloud Properties		Non-drizzle (s.d.)	Drizzle (s.d.)	All Clouds (s.d.)
N_d (CAS) [cm^{-3}]	1 sec	36 (36)	26 (18)	28 (30)
	10 sec	43 (40)	25 (16)	26 (30)
N_d (CIP) [cm^{-3}]	1 sec	0.007 (0.030)	0.18 (0.28)	0.09 (0.21)
	10 sec	0.002 (0.01)	0.22 (0.32)	0.090 (0.217)
r_{eff} (CAS) [μm]	1 sec	10.6 (3.5)	13.5 (2.5)	12.5 (2.9)
	10 sec	9.5 (3.2)	13.6 (2.4)	12.9 (2.8)
r_{effT} (CAS + CIP) [μm]	1 sec	11 (3.9)	32.8 (33)	21.6 (25.7)
	10 sec	9.8 (3.5)	34.4 (28)	22 (27.5)
LWC (CAS) [gkg^{-1}]	1 sec	0.126 (0.151)	0.185 (0.179)	0.146 (0.167)
	10 sec	0.109 (0.119)	0.172 (0.152))	0.139 (0.170)
LWC (CIP) [gkg^{-1}]	1 sec	0.002 (0.008)	0.244 (1.206)	0.122 (0.867)
	10 sec	0.001 (0.003)	0.271 (0.578)	0.122 (0.932)
Temp [°C]	1 sec	-2.8 (6.0)	-0.5 (3.9)	-1.7 (5.2)
	10 sec	-1.8 (5.5	0.5 (3.2)	-3.9 (6.4)

890

Table 3. Summary of microphysical properties of 1 and 10 s consistent drizzle and non-drizzle sections of clouds from 20 flights' observations of three consecutive winters (Jun - Oct, 2013 - 2015). The standard deviations (s.d.) are indicated in parentheses.

895

Table 4. Comparison of thermodynamic and microphysical properties and meteorology from the soundings for two non-drizzle dominant cases (CASES A and B, 23 July 2013 and 01 October 2015, respectively) and two drizzle dominant cases (CASES C and D, 28 June 2013 and 30 August 2015, respectively).

Category	Non-drizzle dominant flights		Drizzle dominant flights	
	CASE A (20130723)	CASE B (20151001)	CASE C (20130628)	CASE D (2015830)
Time in liq. clouds [s]	679	803	1,338	1,754
Drizzle %	0 %	4 %	85 %	91 %
Cloud top	1.2 km	1.8 km	1.6 km	1.5 km
Cloud base	0.8 km	1 km	0.7 km	0.7 km
CTT	-0.3 ºC	0.7 ºC	-2 ºC	-2.6 ºC
CBT	0.2 ºC	5.9 ºC	0.7 ºC	0.1 ºC
In cloud lapse rate	1.7 ºC / km	8.7 ºC / km	5.4 ºC / km	3 ºC / km
Inv. strength	5.5 ºC	3 ºC	2 ºC	7 ºC
Inv. height	0.9 km	1.5 km	1.4 km	1.4 km
Wind direction	S	SW	SW	SE
N_d [cm^{-3}] (s.d.)	89 (37.5)	80 (45.4)	21 (14)	13 (9.7)
r_{eff} [µm] (s.d.)	8.2 (1.2)	8.5 (2)	14.2 (2.4)	13.2 (2.3)
r_{effT} [µm] (s.d.)	8.2 (1.2)	8.5 (10.9)	23 (10.9)	36 (10.9)
LWC (CAS) [gkg^{-1}] (s.d.)	0.165 (0.122)	0.172 (0.199)	0.190 (0.181)	0.079 (0.101)
LWC (CAS+CIP) [gkg^{-1}] (s.d.)	0.165 (0.141)	0.173 (0.210)	0.306 (0.203)	0.390 (0.210)
Synoptic condition	high pressure ridge	post frontal	weak high pressure ridge	associated with low pressure system
MCC[1]	stratiform closed MCC	closed MCC[2]	open MCC	open MCC

The standard deviations (s.d.) are indicated in parentheses for the cloud microphysical properties.

[1] MCC (mesoscale cellular convection). [2] The interpretation of the MODIS image of this day is difficult due to the presence of multi-level clouds.